



HAL
open science

Profile variability of the H α and H β broad emission lines in NGC 5548

A. I. Shapovalova, V. T. Doroshenko, N. G. Bochkarev, A. N. Burenkov, L. Carrasco, V. H. Chavushyan, Suzy Collin, J. R. Valdes, N. Borisov, Anne-Marie Dumont, et al.

► **To cite this version:**

A. I. Shapovalova, V. T. Doroshenko, N. G. Bochkarev, A. N. Burenkov, L. Carrasco, et al.. Profile variability of the H α and H β broad emission lines in NGC 5548. *Astronomy and Astrophysics* - A&A, 2004, 422, pp.925-940. hal-03732443

HAL Id: hal-03732443

<https://hal.science/hal-03732443>

Submitted on 4 Sep 2022

HAL is a multi-disciplinary open access archive for the deposit and dissemination of scientific research documents, whether they are published or not. The documents may come from teaching and research institutions in France or abroad, or from public or private research centers.

L'archive ouverte pluridisciplinaire **HAL**, est destinée au dépôt et à la diffusion de documents scientifiques de niveau recherche, publiés ou non, émanant des établissements d'enseignement et de recherche français ou étrangers, des laboratoires publics ou privés.

Profile variability of the H α and H β broad emission lines in NGC 5548^{*,**}

A. I. Shapovalova^{1,5}, V. T. Doroshenko^{2,7}, N. G. Bochkarev², A. N. Burenkov^{1,5}, L. Carrasco³, V. H. Chavushyan³,
S. Collin⁴, J. R. Valdés³, N. Borisov¹, A.-M. Dumont⁴, V. V. Vlasuyk¹, I. Chilingarian²,
I. S. Fioktistova¹, and O. M. Martinez⁶

¹ Special Astrophysical Observatory of the Russian AS, Nizhnij Arkhyz, Karachaevo-Cherkesia 369167, Russia
e-mail: ashap@sao.ru

² Sternberg Astronomical Institute, University of Moscow, Universitetskij Prospect 13, Moscow 119899, Russia

³ Instituto Nacional de Astrofísica, Óptica y Electrónica, INAOE, Apartado Postal 51 y 216, 7200 Puebla, Pue., Mexico

⁴ LUTH, Observatoire de Paris, Section de Meudon, place Janssen, 92195 Meudon, France

⁵ Isaac Newton Institute of Chile, SAO Branch, Russia

⁶ Benemérita Universidad Autónoma de Puebla, Facultad de Ciencias Físico-Matemáticas, Apdo. Postal 1152,
CP 72000 Puebla, Pue., Mexico

⁷ Isaac Newton Institute of Chile, Crimean Branch, Ukraine

Received 10 November 2003 / Accepted 26 April 2004

Abstract. Between 1996 and 2002, we have carried out a spectral monitoring program for the Seyfert galaxy NGC 5548 with the 6 m and 1 m telescopes of SAO (Russia) and with the 2.1 m telescope of Guillermo Haro Observatory (GHO) at Cananea, Mexico. High quality spectra with $S/N > 50$ in the continuum near H α and H β were obtained, covering the spectral range $\sim(4000\text{--}7500)$ Å with a (4.5 to 15) Å-resolution. We found that both the flux in the lines and the continuum gradually decreased, reaching minimum values during May–June 2002. In the minimum state, the wings of H β and H α became extremely weak, corresponding to a Sy1.8 type, not to a Sy1, as observed previously when the nucleus was brighter. The line profiles were decomposed into variable and constant components. The variable broad component is well correlated with the continuum variation. It consists of a double peaked structure with radial velocities $\sim\pm 1000$ km s⁻¹ relative to the narrow component. A constant component, whose presence is independent of the continuum flux variations, shows only narrow emission lines. The mean, rms, and the averaged over years, observed and difference line profiles of H β and H α reveal the same double peaked structure. The relative intensity of these peaks changes with time. During 1996, the red peak was the brightest, while in 1998–2002, the blue peak became the brighter one. Their radial velocities vary in the $\sim(500\text{--}1200)$ km s⁻¹ range. In 2000–2002 a distinct third peak appeared in the red wing of H α and H β line profiles. The radial velocity of this feature decreased between 2000 and 2002: from the observed profiles, from $\sim+(2500\text{--}2600)$ km s⁻¹ to $\sim+2000$ km s⁻¹ and is clearly seen on the difference profiles. The fluxes of the various parts of the line profiles are well correlated with each other and also with the continuum flux. The blue and red parts of the line profiles at the same radial velocities vary in an almost identical manner. Shape changes of the different parts of the broad line are not correlated with continuum variations and, apparently, are not related to reverberation effects. Changes of the integral Balmer decrement are, on average, anticorrelated with the continuum flux variations. This is probably due to an increasing role of collisional excitation as the ionizing flux decreases. The behavior of the Balmer decrement of the various parts of the line profiles was different in 1996–2000 as compared with the 2001 behavior. Our results favor the formation of the broad Balmer lines in a turbulent accretion disc with large and moving “optically thick” inhomogeneities, capable of reprocessing the central source continuum.

Key words. galaxies: active – galaxies: Seyfert – galaxies: individual: NGC 5548 – line: profiles

1. Introduction

An important question in the study of active galactic nuclei (AGN) is the nature of the “central engine”. A popular assumption is that the nuclear activity is caused by accretion of gas onto a supermassive black hole (Rees 1984; Begelman 1985). The basic energy release of an AGN occurs very close to the nucleus ($r < 0.001$ pc), as an UV and X-ray

* Appendices A and B are only available in electronic form at <http://www.edpsciences.org>

** Tables 2 and 5 are only available in electronic form at the CDS via anonymous ftp to cdsarc.u-strasbg.fr (130.79.128.5) or via <http://cdsweb.u-strasbg.fr/cgi-bin/qcat?J/A+A/422/925>

continuum most probably produced by a geometrically thin accretion disc. Then, broad emission lines are produced in a zone (the BLR) that reprocesses a fraction of the central UV-X continuum. A zone located further out ($r > 0.001$ pc). The BLR is filled with gas obviously linked with the accretion process. It is therefore important to know its structure and kinematics, in order to gain insight into the central engine. However, even for nearby objects, the typical angular size of the BLR corresponds to <0.001 arcsec, hence we will have to wait for the availability of more sensitive optical interferometers to resolve it. Fortunately, another methods exist to study the BLR structure.

It is well known that AGNs vary in luminosity on time scales from years to hours, over the entire wavelength range from radio to X-ray or γ -ray. In particular, the flux in the broad emission lines varies in response to changes in the ionizing continuum with short time delays (days to weeks for Seyfert galaxies), due to light-travel time effects within the BLR. If the BLR gas has systematic motions such as infalling, outflowing, circular motions, etc., then the profiles of the broad emission lines must vary in a way related with the geometry and the kinematics of the gas in this region, and with the processes of gas relaxation that follow the changes in the ionizing flux (Bahcall et al. 1972; Bochkarev & Antokhin 1982; Blandford & McKee 1982; Antokhin & Bochkarev 1983).

Studying the correlations between the flux changes in the continuum and in the broad emission line profiles, one can obtain a “map” of the geometrical and dynamical structure of the BLR. This method is known as “Reverberation mapping” (see Peterson 1993, and references therein). Important progress in the understanding of the BLRs was achieved as a result of multiwavelength monitoring campaigns within the framework of the “International AGN Watch”, a consortium organized to study several Seyfert galaxies (Peterson et al. 1999). A large amount of data has been obtained in the multiwavelength monitoring of the Seyfert 1 galaxy NGC 5548, including its continuous monitoring in the optical range for 13 years (1988–2001) (Clavel et al. 1991; Peterson et al. 1991, 1994, 1999, 2002; Dietrich et al. 1993; Korista et al. 1995). These investigations have given the following results:

1. The response time of the H β line to continuum variations varies from year to year (from ~ 8 to 26 days) and it is correlated with the average continuum flux.
2. The high ionization lines have shorter response times to continuum variations than the low ionization ones, indicating the presence of ionization stratification along the radius of the broad line region.
3. The optical and ultraviolet continua vary almost simultaneously (i.e. without showing a significant delay).
4. The UV/optical continuum becomes “harder” as it gets brighter.

The results of the study of the radial velocity field in the BLR of NGC 5548 are still ambiguous. The analysis of the “AGN Watch” spectra reveals a complex behaviour. Crenshaw & Blackwell (1990) found that the red wing of C IV λ 1550 responds faster to changes of the continuum than the blue wing does, implying important radial motions (infalling). Later on, Korista (1994) observed that both wings presented the same

delay with respect to continuum light variations, implying Keplerian rotation or turbulent symmetrical motions. The absence of important radial motions in the BLR was further confirmed by the analysis of the transfer function (TF) of the H β (Wanders & Peterson 1996) and C IV λ 1550 (Wanders et al. 1995) emission lines. It was also found that the broad wings of the emission lines respond faster to continuum variations than the line cores (Clavel et al. 1991; Korista 1994; Korista et al. 1995; Kollatschny & Dietrich 1996; Wanders & Peterson 1996). In several studies, the presence of a multi-component structure of the BLR with distinct physical characteristics is required to account for the observed broad line profile variability in this object (Peterson 1987; Stirpe et al. 1988; Stirpe & de Bruyn 1991; Sergeev et al. 1994; Wanders & Peterson 1996). Consequently, the observed profiles in NGC 5548 have been interpreted in the framework of different models, such as: binary black holes (Peterson et al. 1987), accretion disc (Stirpe et al. 1988; Rokaki & Boisson 1999), BLR from the clouds rotating about the massive central gravitational source in occasionally inclined Keplerian orbits and illuminated by an anisotropic continuum source (Wanders et al. 1995; Wanders & Peterson 1996).

Further study of the broad emission line profile changes on longer time scales, may allow us to prove or disprove some of the previously advanced hypothetical scenarios. This is the purpose of the present paper.

In this paper we present the results of an optical spectral study of NGC 5548 for the 1996–2001 period, including part of our 2002 data (see Sect. 2.1). Some partial results of our monitoring campaign were reported earlier (Shapovalova et al. 2001a,b, 2002). In Sect. 2, we discuss the observations and data processing. In Sect. 3 we present the analysis of the H β and H α line profile variability. The decomposition of the profiles into constant and variable components, the mean and rms spectra, are discussed. The behaviour of the radial velocities of spectral features in the broad line profiles, is studied both from the observed profiles and from the difference profiles. We use words “bump” for wide features and “peak” for their tops (maxima). The correlation analysis between fluxes and shapes of the different parts of the line profiles is presented. The behaviour of the Balmer decrement is studied. In Sect. 4, we summarize our results and compare them with those of other researchers. Possible interpretations are discussed in Sect. 5, and conclusions are listed in Sect. 6. In Appendix A, a modified spectrum scaling method adopted in this paper is presented.

Note that all these data are also included in the AGN Watch database and are publicly available.

2. Observations and data reduction

2.1. Optical Spectroscopy

We report the spectral observations of NGC 5548 carried out between 1996 Jan. 14 (Julian date = JD 2450097) and 2001 Aug. 9 (JD 2452131) during 113 nights. Our analysis is based on those spectra. However for the studies described in Sects. 3.1, 3.2.3 and 3.2.4 (for studying the behavior of the peaks and bumps) we have also used spectra taken on June 4, 2002,

Table 1. Sources of spectroscopic observations.

Source	Code	Tel. and equip.	Aperture
1	2	3	4
SAO (Russia)	L1	1 m+UAGS	4.2'' \times 19.8''
SAO (Russia)	L1	1 m+UAGS	8.0'' \times 19.8''
SAO (Russia)	L	6 m+UAGS	2.0'' \times 6.0''
Guillermo Haro	GH	2.1 m+B and C	2.5'' \times 6.0''
Obs. (Mexico)			

Table 2. Log of the spectroscopic observations.

This table is only available in electronic form at the CDS. It contains the following information for 116 dates: Col. 1 – number; 2 – UT date; 3 – Julian date; 4 – code according to Table 1; 5 – projected spectrograph entrance apertures; 6 – wavelength range covered; 7 – spectral resolution; 8 – mean seeing; 9 – position angle (PA) in degrees; 10 – signal to noise ratio in the continuum (5160–5220) Å near H β and (6940–7040) Å near H α .

and May 15, 17, 2002, when NGC 5548 was in a minimum activity state and the 2002 annual averages of both the observed and difference profiles for H α and H β .

Optical spectra of NGC 5548 were obtained with the 6 m and 1 m telescopes of SAO (Russia, 1996–2002) and at INAOE's 2.1 m telescope at the Guillermo Haro Observatory (GHO) at Cananea, Sonora, Mexico (1998–2002). These were obtained with long slit spectrographs equipped with CCDs. The typical wavelength range covered was from 4000 Å to 7500 Å, the spectral resolution was 4.5–15 Å, and the S/N ratio was >50 in the continuum near H α and H β . Spectrophotometric standard stars were observed every night. The informations on the source of spectroscopic observations are given in Table 1: 1 – the source (Observatory); 2 – a code assigned to each telescope+equipment, used throughout this paper (the code was chosen in accordance with the monitoring campaigns of NGC 5548 (Dietrich et al. 2001; Peterson et al. 2002); 3 – the telescope aperture and the spectrograph; 4 – the projected spectrograph entrance apertures (the first dimension is the slit-width, and the second one is the slit-length).

The spectrophotometric data reduction was carried out either with the software developed at the SAO RAS by Vlasyuk (1993), or with IRAF for the spectra obtained in Mexico. The image reduction process included bias subtraction, flat-field corrections, cosmic ray removal, 2D wavelength linearization, sky spectrum subtraction, stacking of the spectra for every setup, and flux calibration based on standard star observations.

2.2. Absolute calibration of the spectra

Even under good photometric conditions, the accuracy of spectrophotometric measurements is rarely better than 10%. Thus the standard technique of flux calibration, by means of comparison with stars of known spectral energy distribution, is not good enough for the study of AGN variability. Instead, we use the fluxes of the narrow emission lines which are known to be non-variable on time scales of tens of years in most AGN.

Consequently, the bright narrow emission lines can be adopted as internal calibrators for scaling AGN spectra (Peterson 1993). So, we assume that the flux of the [O III] λ 5007 line remains constant during the interval covered by our observations. All blue spectra of NGC 5548 are scaled to a constant flux value of $F([\text{O III}]\lambda 5007) = 5.58 \times 10^{-13} \text{ erg s}^{-1} \text{ cm}^{-2}$ determined by Peterson et al. (1991) and corrected for aperture effects as described below. The scaling of the blue spectra was carried out using a variation on the method of Van Groningen & Wanders (1992), described in Appendix A. This method allows to obtain a homogeneous set of spectra with the same wavelength calibration and the same [O III] λ 5007 flux value.

The spectra obtained with the GHO 2.1 m telescope (Mexico) with a resolution of 15 Å. They contain both the H α and H β regions, and were scaled using the [O III] λ 5007 line.

Most of spectra from the 1 m and 6 m SAO telescopes were obtained separately in the blue (H β) and red (H α) wavelength intervals, with a resolution of 8–9 Å. Usually, the red edge of the blue spectra and the blue edge of the red spectra overlap in an interval of ~ 300 Å. Therefore, the most of the red spectra were scaled using the overlapping continuum region with the blue ones, which were scaled with the [O III] line. In these cases the scaling uncertainty is about 5%.

However, for 10 red spectra the scaling of the continuum by this method was not possible, this due to several reasons: ie. some spectra were obtained with a higher resolution (~ 5 Å) and did not overlap with the blue spectra; or the some spectrum ends were distorted by the reduction procedure; or blue spectra were not taken on that night. These 10 spectra were scaled using the integral flux in the narrow emission lines in the H α , region: [N II] $\lambda\lambda$ 6548, 6584 and [S II] $\lambda\lambda$ 6717, 6731. To this purpose, on the red spectra we located a linear continuum through points that are free from the absorption lines (6120 Å and 7020 Å) in 20 Å windows.

After continuum subtraction, we obtained the best gaussian fit to the H α profile through a blend of 7 emission components: very broad H α ($FWHM \sim 10\,000 \text{ km s}^{-1}$), blue broad H α , red broad H α , narrow H α , [N II] $\lambda\lambda$ 6548+6583 (double gaussian function with $I(6584)/I(6548) = 3$), [S II] λ 6717 and [S II] λ 6731. Figure 1 shows an example of a Gaussian fit to the H α blend.

Table 3 lists our mean values of the flux in the narrow components derived from the scaled red spectra, jointly with the result obtained by Dietrich et al. (1993) from the spectra taken in 1988–1989. These authors obtained a good Gaussian fit to H α with only 5 components: namely, very broad H α , broad H α , narrow H α , [N II] $\lambda\lambda$ 6548, 6584. With our spectra we tried to carry out a similar fitting to the same 5 components, but we ended up with large residuals (~ 10 – 20%) in the region where the blue and red bumps appear. Apparently, on the spectra in Dietrich et al. (1993), such features were not as bright as in our spectra. However, in any profile fit, the narrow components should remain constant.

We can see on Table 3 that the fluxes obtained for the narrow lines are consistent within the errors with the values obtained by Dietrich et al. (1993). Using the integral fluxes for the narrow lines from Table 3 we scaled the 10 red spectra.

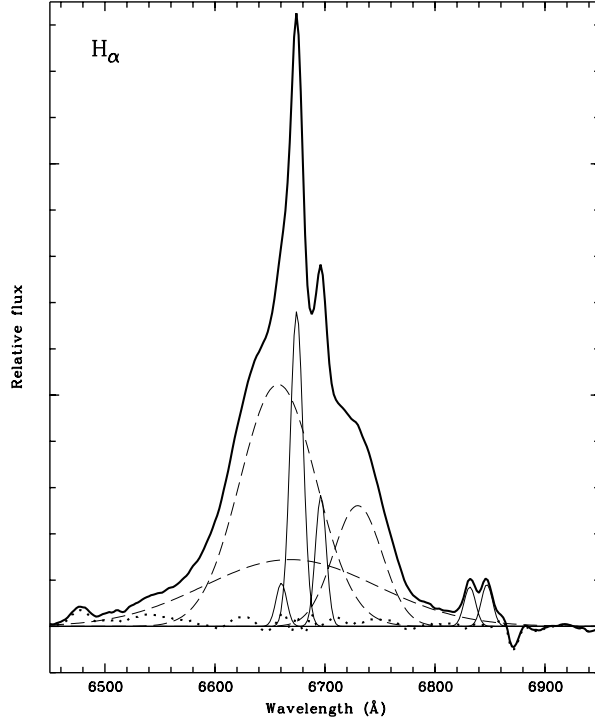


Fig. 1. Gaussian deconvolution of the H α blend in several components; thick solid line: the observed profile; thin solid line: the narrow component of H α , [N II] $\lambda\lambda$ 6548, 6584, [S II] $\lambda\lambda$ 6717, 6731; dashed line: very broad, blue broad, and red broad components of H α ; points: the residual of the observed profile and the sum of all gaussian components. Our analysis do not include a small hump in the left side ([O I] λ 6364).

Table 3. Fluxes of H α Gaussian components.

Component	Flux*	
	Mean (GHO+SAO)	Dietrich et al. (1993)
H α _{narrow}	0.350 \pm 0.040	0.344 \pm 0.045
[N II] $\lambda\lambda$ 6548, 6584	0.160 \pm 0.036	0.182 \pm 0.022
[S II] $\lambda\lambda$ 6717, 6731	0.097 \pm 0.021	
Sum (H α _{narrow} , [N II])	0.510 \pm 0.054	0.526 \pm 0.050
Sum narr. all	0.607 \pm 0.064	

* $F([\text{O III}]\lambda 5007) = 1.0$.

2.3. Intercalibration of the spectral data

From the scaled spectra we determined the average flux in the continuum at the observed wavelength ~ 5190 Å (or at ~ 5100 Å in the rest frame of NGC 5548, $z = 0.0167$), by means of flux averages in the bandpass (5180–5200) Å. For the determination of the observed fluxes of H β and H α , it is necessary to subtract the continuum. To this goal, a linear continuum was located through windows of 20 Å located at 4790 Å and 5170 Å for the H β region, and at 6120 Å and 7020 Å for the H α region. After the continuum subtraction, we defined the observed fluxes in the lines in the following wavelength intervals: (4795–5018) Å for H β (the interval is similar to that in Peterson et al. 2002),

Table 4. Flux scale factors for optical spectra.

Sample	Aperture	Point-source	Extended source
		scale factor	correction
		φ	G^*
L1	4.2'' \times 19.8''	1.000	0.000
L1	8.0'' \times 19.8''	1.089 \pm 0.031	0.84 \pm 0.45
GH	2.5'' \times 6.0''	1.009 \pm 0.021	-2.76 \pm 0.11
L	2.0'' \times 6.0''	1.036 \pm 0.048	3.85 \pm 0.86

* In units of 10^{-15} erg s $^{-1}$ cm $^{-2}$ Å $^{-1}$.

and (6500–6800) Å for H α (the interval is like that in Dietrich et al. 2001).

All fluxes were corrected for aperture effects because, while the BLR and non-stellar continuum are effectively point-like sources ($\ll 1''$), the NLR is an extended one ($> 2''$). Consequently, the measured NLR flux depends on the size of the spectrograph's entrance aperture (see Peterson et al. 1995, for a detailed discussion). In order to correct our fluxes for aperture effects, we determined a point-source correction factor (φ) given by:

$$F(\text{H}\beta) = \varphi \cdot F_{\lambda 5007} \left(\frac{F(\text{H}\beta)}{F([\text{O III}]\lambda 5007)} \right)_{\text{obs}}, \quad (1)$$

where $F_{\lambda 5007}$ is the absolute flux in the [O III] λ 5007 line, and the value in brackets is the H β to [O III] λ 5007 observed flux ratio.

The light contribution of the host galaxy to the continuum depends also on the aperture size. The continuum fluxes $F_{\lambda}(5190)$ were corrected for different amounts of host-galaxy contamination, according to the following expression (see Peterson et al. 1995):

$$F_{\lambda}(5190 \text{ \AA}) = \varphi \cdot F_{\lambda 5007} \left(\frac{F_{\lambda}(5190 \text{ \AA})}{F([\text{O III}]\lambda 5007)} \right)_{\text{obs}} - G, \quad (2)$$

where $F_{\lambda 5007}$ is the absolute flux in the [O III] λ 5007 line and the value in brackets is the continuum to [O III] λ 5007 observed flux ratio, G being an aperture dependent correction factor to account for the host galaxy light. The case L1 (Table 1), which corresponds to a relatively large aperture (4.2'' \times 19.8''), was adopted as a standard (i.e. $\varphi = 1.0$, $G = 0$ by definition). The corrections φ and G were defined for every aperture via the comparison of a pair of observations separated in time by 1–3 days. This means that the real variability on shorter times (< 3 days) will be suppressed by the procedure of data recalibration. Point-source correction factors φ and G values for various samples are given in Table 4. Using these factors, we recalibrate the observed fluxes in the lines and continuum to a common scale corresponding to an aperture of 4.2'' \times 19.8''.

The fluxes listed in Table 5 were not corrected for the contributions of the narrow-line emission components of H β , H α , and [N II] $\lambda\lambda$ 6548, 6584. These are constant and should not influence a broad line variability study. The mean error (uncertainty) in our flux determination for both, the H β and the continuum, is $\sim 3\%$, while it is $\sim 5\%$ for H α . These quantities were estimated by comparing our results from the spectra obtained within time intervals shorter than 3 days.

Table 5. Observed continuum, H β and H α fluxes.

Table 5, where we list our results of fluxes measurement, is only available in electronic form at the CDS and contains the following information. Columns: 1 – UT-date; 2 – Julian date; 3 – a telescope code, according to Table 1; 4 – $F(\text{cont})$, the continuum flux at 5190 Å (in units of 10^{-15} erg s $^{-1}$ cm $^{-2}$ Å $^{-1}$), reduced to the 1 m telescope aperture $4.2'' \times 19.8''$; 5 – ε_c , the estimated continuum flux error; 6 – $F(\text{H}\beta)$, the H β total flux (in units of 10^{-13} erg s $^{-1}$ cm $^{-2}$); 7 – $\varepsilon_{\text{H}\beta}$, the H β flux error; 8 – $F(\text{H}\alpha)$, the H α total flux (in units of 10^{-13} erg s $^{-1}$ cm $^{-2}$); 9 – $\varepsilon_{\text{H}\alpha}$, the H α flux error.

2.4. Subtraction of the narrow emission line contribution

In order to study the broad components of hydrogen lines showing the main BLR characteristics, one must remove the narrow component of these lines and the forbidden lines from the spectra. To this purpose, we constructed spectral templates for the H β and the H α blends using a Gaussian fit to the higher spectral resolution (~ 8 Å) profiles observed near the minimum light state (for details see Sect. 2.2 and Fig. 1). The obtained template spectra are the sum of the following gaussian components: for H β , the narrow component of H β , [O III] $\lambda\lambda$ 4959, 5007; for H α , the narrow component of H α , [N II] $\lambda\lambda$ 6548, 6584 and [S II] $\lambda\lambda$ 6717, 6731. The flux values obtained for the narrow components of H β and H α in the template spectra are: $F(\text{H}\beta)_n = (0.131 \pm 0.012)F(\lambda 5007)$; $F(\text{H}\alpha)_n = (0.398 \pm 0.02)F(\lambda 5007)$, respectively. Then, we scaled the blue and red spectra according to our scaling scheme (see Appendix A), taking the template spectrum as a reference. Our template spectrum and any individual observed spectrum are thus matched in wavelength, reduced to the same resolution, and then subtracted from one another. After subtraction of the narrow components, the spectra of the H α and H β broad lines is reduced to the aperture $4.2'' \times 19.8''$ (Eq. (1)), using φ values listed in Table 4 (Sect. 2.3).

Since the scaling is done from the line [O III] λ 5007, we had to use the $FWHMs$ obtained from the corresponding blue spectrum to reduce the H α region. But the $FWHM$ of [N II] $\lambda\lambda$ 6548, 6584 and [S II] $\lambda\lambda$ 6717, 6731 lines is usually somewhat smaller (by ~ 5 – 10%) than the $FWHM$ of [O III] λ 5007. Therefore, the subtraction of these components is rather poor when one has large spectral resolution differences between the template and individual spectra.

Another way to remove the narrow emission lines, consists in subtracting the spectra from each other, i.e. obtaining difference spectra. The H β and H α difference profiles are thus obtained by subtracting the minimum activity state spectrum from the individual spectra. For a good subtraction, it is necessary for the spectra to have similar spectral resolution. These questions are solved via the method mention in Appendix A, where a spectrum in minimum state is used as a reference spectrum. The difference spectra will be discussed hereinafter.

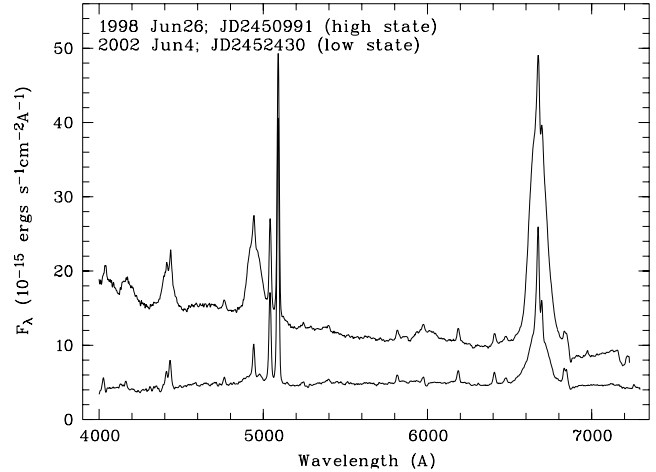


Fig. 2. The spectra of NGC 5548 corresponding to the high activity state (*top*) and to the low activity state (*bottom*). The abscissae give the observed wavelengths ($z = 0.0167$). The ordinates give the fluxes in units of 10^{-15} erg cm $^{-2}$ s $^{-1}$ Å $^{-1}$.

3. Data analysis

3.1. Variability of H β and H α emission lines and of the optical continuum

In Table 5 it is apparent that both, the continuum and permitted line emission fluxes, decreased continuously from maximum values in 1998 to minimum ones in 2002. The maximum amplitude ratios of the flux variations during this period were: for H β line – ~ 4.7 ; for H α – ~ 3.4 ; and for the $\lambda 5190$ Å continuum – ~ 2.5 . Photometric data by Doroshenko et al. (2001) and Spiridonova (2002) also yield a maximum amplitude of the flux variations ratio ~ 2.5 in the V band in this period. Thus, the variations inferred from the spectral and broad band photometry of the continuum are in excellent agreement. This fact is in turn indicative of a constant flux in the line [O III] λ 5007, a key assumption in our spectral scaling scheme. It is worth mentioning, that the galactic bulge light contribution to our spectra was not subtracted. Therefore, the derived maximum amplitude ratio for the continuum flux changes is, consequently, smaller than the ones derived for emission lines. In 2002, the flux in the lines and continuum reached a minimum value by mid May or early June. In Fig. 2 we plot spectra of the high and low activity states, obtained in June 26, 1998, and June 4, 2002, respectively. There one can see that in the low activity state, the flux in the continuum decreased by a large factor (~ 2.5 times), while the slope of the continuum in the blue, became significantly flatter, showing a spectral index > 2 to be compared with the ~ 1.0 a value observed at the high activity state. Also, at minimum activity state, the emission wings of H β and H α became extremely weak. These profiles correspond to a Sy1.8 type and not to a Sy1, as observed in maximum light (i.e. the spectral type of the object had suffered a dramatic change!).

In Fig. 3 we present the light curves of the H β and the H α emission lines and the combined continuum. The flux in the lines and spectral continuum are those listed in Table 5. The combined continuum data includes both the $\lambda 5190$

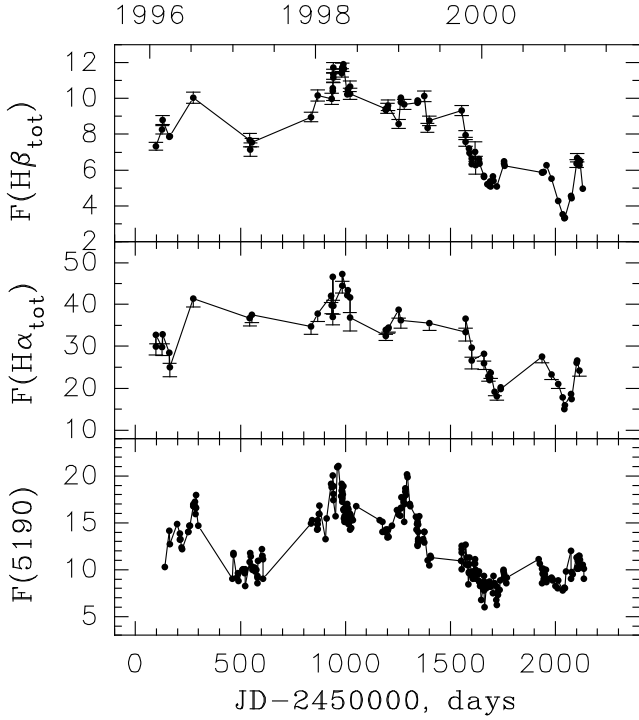


Fig. 3. The light curves of $H\beta$, $H\alpha$, and the continuum at the observed wavelength $\lambda 5190 \text{ \AA}$. The narrow components were not subtracted. Fluxes in lines are in units of $10^{-13} \text{ erg cm}^{-2} \text{ s}^{-1}$, and in continuum in $10^{-15} \text{ erg cm}^{-2} \text{ s}^{-1} \text{ \AA}^{-1}$. The continuum is the “combined continuum” obtained from the spectra and photometric points in the V band in 1996–2001.

spectral data and some V band photometry from Doroshenko et al. (2001) and Spiridonova (2002). The V band data were converted into $\lambda 5190$ continuum flux values through the expression given by Dietrich et al. (2001):

$$\log F_{\lambda}(5500) = -0.4 m_V - 8.439. \quad (3)$$

A comparison of the spectral continuum at $\lambda 5190 \text{ \AA}$, $F_c(\lambda 5190)$ with some simultaneous observations made in the V band leads to the following transformation equation:

$$F_c(\lambda 5190) = (1.120 \pm 0.064) \times F_{\lambda}(V) - (0.608 \pm 0.776), \quad (4)$$

(correlation coefficient $r = 0.95$). Here the fluxes are given in units of $10^{-15} \text{ erg cm}^{-2} \text{ s}^{-1} \text{ \AA}^{-1}$. One sees in Fig. 3 that the $H\beta$ and $H\alpha$ fluxes vary approximately in the same way. We have compared our light curves of H-beta and of the continuum with those obtained by Peterson et al. (2002) from the AGN-Watch program. The comparison shows that our H-beta fluxes coincide within the uncertainties with the AGNW data. The continuum fluxes differ because of the different apertures, which are $4.2'' \times 19.8''$ for our data and $5.0'' \times 7.5''$ for the AGNW data. The correction for the different apertures necessary to convert our data to Peterson et al.’s data (2002) is $F(\text{cnt})_{\text{pet.}} = F(\text{cnt})_{\text{our}} - 2.5$ (the fluxes are in units $10^{-15} \text{ erg cm}^{-2} \text{ s}^{-1} \text{ \AA}^{-1}$). With the introduction of such a correction, our continuum fluxes coincide with the AGNW data within the uncertainties.

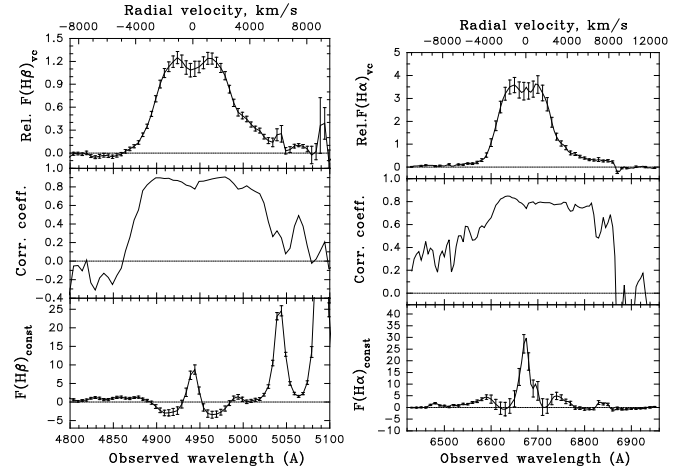


Fig. 4. The $H\beta$ (left) and $H\alpha$ (right) profile decomposition of the variable (top) and constant (bottom) components. The flux of the constant components is in units $10^{-15} \text{ erg cm}^{-2} \text{ s}^{-1} \text{ \AA}^{-1}$. For the variable components, the relative increment of the line flux when the continuum flux increases by an amount of $1 \times 10^{-15} \text{ erg cm}^{-2} \text{ s}^{-1} \text{ \AA}^{-1}$ is shown. The correlation coefficient between the variable component of lines and the continuum flux at different wavelengths along the line profile is shown in the middle panels.

3.2. $H\alpha$ and $H\beta$ profile variations

3.2.1. $H\beta$ and $H\alpha$ profile decomposition

As shown by Sergeev et al. (1994), if a line profile is composed of only a variable and a constant part, it is possible to separate these components. The constant component is present in the form of narrow emission lines, which are formed far away from the nucleus and are independent of changes in the continuum emitted by the central source. The variable component is formed in the BLR and is strongly dependent on the flux of the central source through reverberation. We have applied the two-component profile decomposition method to spectra obtained in 1996–2001. We assume that the fluxes in the variable part of the emission lines are correlated linearly with the continuum flux, as shown by Peterson et al. (2002, Fig. 3). An underlying continuum was subtracted from each of the scaled spectra. The region occupied by an emission line is divided into equidistant narrow spectral intervals (5 \AA bins). For every bin a light curve is constructed. A linear regression for each of these light curves and that of the continuum was computed. This is done by taking into account the mean delay time between them (~ 20 days, Peterson et al. 2002). The introduction of the more precise time delays obtained for each year by Peterson et al. (2002) for $H\beta$ does not change the profile shape of the variable component, within the errors marked in Fig. 4. Since the exact year-averaged time delay for $H\alpha$ is not known, we used the same average time delay for the both lines. The variable part in the profile is computed as the increment of line flux per unit flux increase of the continuum. The non-variable part of the profile is estimated by the extrapolation of the line flux in every bin to a zero continuum flux value.

This scheme allows us to separate the part of the line profiles that is linearly related to the continuum light changes from

those which remain constant in time. It also provides a scheme to estimate the H β and H α narrow line fluxes in an independent way from that described in Sect. 2.4. In any case both methods yielded very similar results.

Figure 4 shows the variable (top) and constant (bottom) components of the H β (left) and H α (right) lines. The correlation coefficient of the variable component with the continuum across the emission lines is plotted in the central panels. Both variable components present a double-peaked structure with maxima at radial velocities $\sim\pm 1000$ km s $^{-1}$. The variable part of the H β and H α profiles between ~-4000 km s $^{-1}$ and $\sim+5000$ km s $^{-1}$ show a highly correlated ($r \sim 0.8$) response to changes in the continuum. The constant component panels contain mainly the narrow line emission of H β , [O III] λ 4959, 5007 Å (left) and of H α , [N II] $\lambda\lambda$ 6548, 6584, [S II] $\lambda\lambda$ 6717, 6731 and [O I] λ 6364 (right).

3.2.2. Mean and root-mean-square spectra

The comparison between an average and root-mean-square (rms) spectrum provides us a good measure of the profile variability. Average and rms H β and H α profiles were calculated after removing the continuum and the narrow lines from the profiles (see Sects. 2.3 and 2.4).

The mean H β and H α profiles and the absolute rms variations per unit wavelength are shown in Fig. 5. It is clear that both profiles present a double-peaked structure with maxima at radial velocities $\sim\pm 1000$ km s $^{-1}$ relative to the narrow components. On the mean and rms H α and H β profiles, a distinct red asymmetry is observed at radial velocities >2000 km s $^{-1}$, the red wing being brighter than the blue one. This is indicative of stronger variability of the red wing as compared to the blue one during the monitoring period.

On the rms H α profile, a small peak is seen at a zero radial velocity, which is caused by an improper subtraction of the narrow H α component for spectra of lower resolution. The *FWHM* value of the mean and rms profiles is ~ 6300 km s $^{-1}$ and ~ 5800 km s $^{-1}$, respectively. These values are close to those obtained by Wandel et al. (1999) from spectra obtained during the 1989–1996. The mean profiles of H β and H α show blue peaks brighter than the red ones during the 1996–2001.

3.2.3. Time evolution of the broad H β and H α profiles

The study of the shape of the broad emission line profiles and their variation in time, can help in choosing a suitable model of the BLR. From our spectra it is seen that within every month, the broad line profile did not vary at a noticeable level. The flux in the lines also varied very slightly (as a rule, by 2–5%, and only in some cases up to 10%). Within every year, the shape of the profile did not vary at a noticeable level, but the fluxes in the broad emission lines varied considerably in 2000–2001. Then averaging the broad profiles over months or years, in order to increase the signal to noise ratios, allows us to see their time evolution in a more reliable way than on the individual spectra. Therefore, for each month and each year, we have obtained the mean profiles.

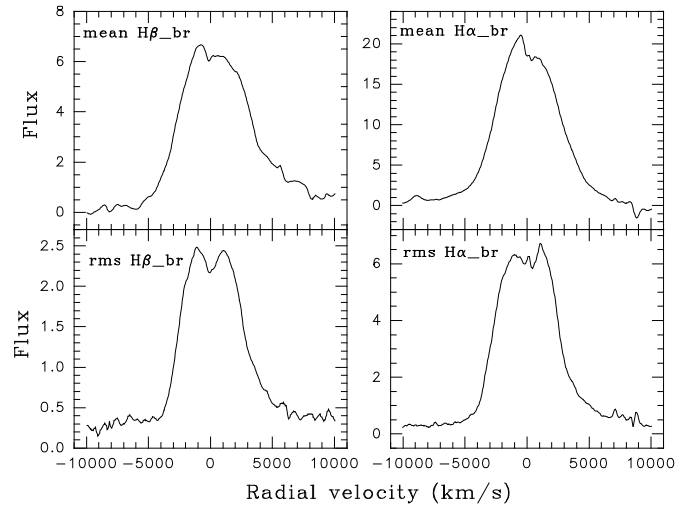


Fig. 5. The mean (*top*) and rms (*bottom*) H β (*left*) and H α (*right*) profiles. The abscissae are the radial velocities relative to the narrow components; the ordinates give the fluxes in units 10^{-15} erg cm $^{-2}$ s $^{-1}$ Å $^{-1}$.

The averaged profiles of H β and H α broad emission lines in subsequent years are shown in Fig. 6. The evolution of the profile is well seen: in 1996, double peaks are present at radial velocities ~-1000 km s $^{-1}$ and $\sim+1200$ km s $^{-1}$; in 1997–1998, the double peaks are distinctly seen at radial velocities of about ± 1000 km s $^{-1}$, and in 1999, they are located at radial velocities of about $\pm(500-900)$ km s $^{-1}$; in 2000–2002, a bright blue peak is still present at $\sim-(700-1000)$ km s $^{-1}$, but on the red side at $\sim+1000$ km s $^{-1}$, a bending shoulder is seen instead of a bump. The relative brightness of the peaks varies: the blue peak was brighter than the red one in 1998–2002; but in 1996, the red peak at a radial velocity of $\sim+1200$ km s $^{-1}$ became brighter. These effects are best seen on the H β profile than on the H α one. It is because the narrow components are not well subtracted in the H α case.

In 2000–2002, a new bright bump is clearly seen in the red wing of the broad lines at a radial velocity of about $\sim+2500$ km s $^{-1}$. In order to investigate whether or not the radial velocity of the new bump varies, we compared the observed profiles of H β obtained at different times (before subtraction of the narrow component). We have measured the radial velocity of the peak of this bump using good spectra with similar resolution (8–9 Å) and a high *S/N* ratio ≥ 50 . We have also used the measurements of the peak location in May, 2003 obtained from the spectra taken with the 6 m telescope. The bump is relative broad, and the determination of the radial velocity of its peak is somewhat uncertain. Using the individual spectra of H β we defined the radial velocities of the bump peak by two methods: 1) as the mean-weighted location of the point in the bump corresponding to the level ~ 0.8 *I*_{max} (*I*_{max} being the maximum of the peak intensity); 2) by fitting the bump top with a parabola. Both methods gave similar results. The only difference is that the second method (fitting by a parabola) gives radial velocities of the bump peak systematically ~ 100 km higher, probably because of the slight blue asymmetry. We think that the first method gives more realistic results. Therefore we present the year-averaged radial velocities of this red peak derived by

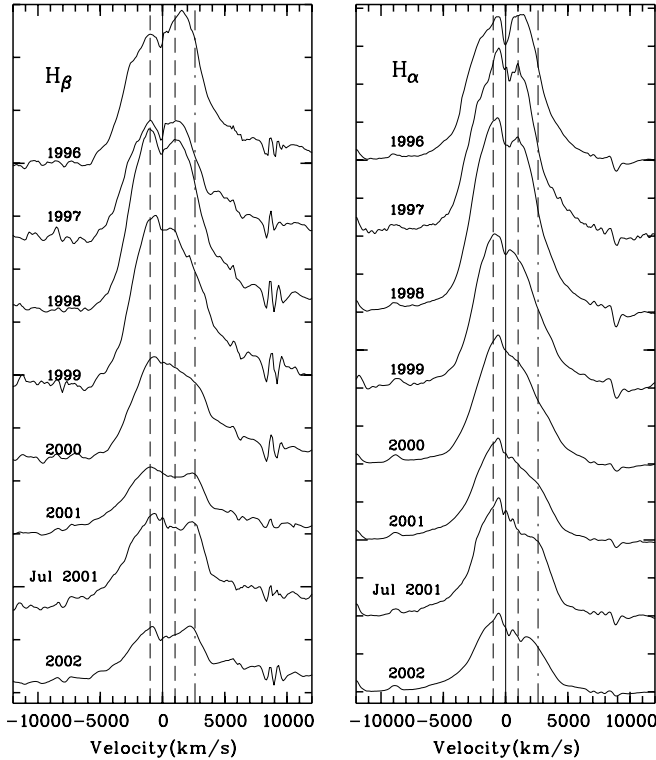


Fig. 6. Annual averages from 1996 to 2002 of the observed profiles of $H\beta$ broad emission component after subtraction of the continuum and the narrow components of $H\beta$ and $[O\text{III}]\lambda\lambda 4959, 5007$ (left). The same for $H\alpha$ after subtraction of the continuum and the narrow components of $H\alpha$, $[N\text{II}]\lambda\lambda 6548, 6584$ and $[S\text{II}]\lambda\lambda 6717, 6731$ (right). The vertical lines correspond to the radial velocities: dashed lines: $\pm 1000\text{ km s}^{-1}$; dash-dot lines: $\sim +2600\text{ km s}^{-1}$; thin line: 0 km s^{-1} . The abscissae give the radial velocities relative to the narrow component of $H\beta$ and $H\alpha$. The ordinates give the relative fluxes. The profiles are shifted vertically by a constant value.

method 1 in Table 6: 1 – year; 2 – the average radial velocity relative to the narrow component of $H\beta$ and the root-mean-square error obtained from measurements on the individual spectra; 3 – the average continuum flux at the observed wavelength 5190 \AA and its dispersion; 4 – the S/N ratio on the average spectrum in the region $(5160\text{--}5220)\text{ \AA}$. One sees clearly on this table that the radial velocity of the peak decreases: in 2000–2001 it corresponds to $\sim(2500\text{--}2600)\text{ km s}^{-1}$, and in 2002–2003 to $\sim 2000\text{ km s}^{-1}$, within the uncertainties. This effect is well seen in Fig. 7, where the year-averaged normalized profiles of $H\beta$, derived by dividing the observed profiles by the average $H\beta$ flux for each year, are presented. A similar result is obtained from the observed profiles after subtraction of the narrow components. Thus, during 3 years (from 2000–2001 to 2002–2003) a considerable shift $\sim 500\text{ km s}^{-1}$ of the red peak is observed on the $H\beta$ profiles.

From Table 6, there is no apparent correlation between the variations of the radial velocities of this peak and the average continuum flux.

Table 6. Year-averaged radial velocity of the new red peak in 2000–2003, derived from the observed $H\beta$ profiles before subtraction of the narrow component.

Year	V_r (km s^{-1})	$F(\text{cont})^*$ 5190 \AA	S/N (5160–5220) \AA
2000	2660 ± 106	9.27 ± 1.28	70
2001	2438 ± 83	9.66 ± 1.26	95
2002	2088 ± 46	7.11 ± 0.98	76
2003	1986 ± 75	10.43	95

* $F(\text{cont})$ in units of $10^{-15}\text{ (erg cm}^{-2}\text{ s}^{-1}\text{ \AA}^{-1})$.

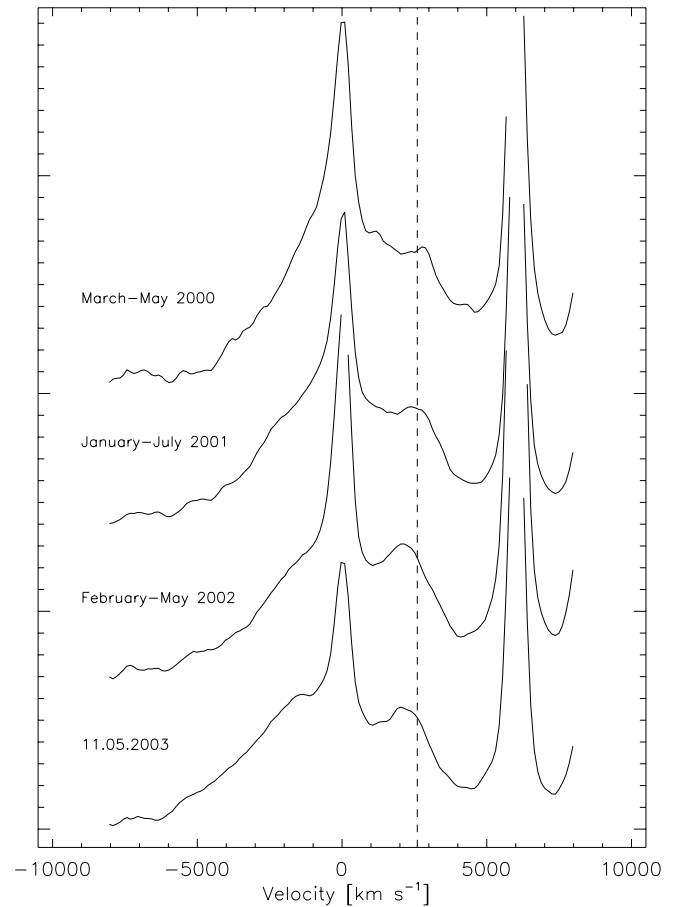


Fig. 7. Year-averaged normalized profiles of $H\beta$ in 2000–2003. The vertical dashed line corresponds to a radial velocity $+2600\text{ km s}^{-1}$. The abscissae give the radial velocities relative to the narrow component of $H\beta$. The profiles are shifted vertically by a constant value.

3.2.4. $H\alpha$ and $H\beta$ difference profiles

For the analysis of the shape changes in the broad line profiles, the best method is that of direct subtraction of spectra, i.e. obtaining the difference spectra. In this case, the narrow emission lines and the absorption lines of the host galaxy, which may distort the observed emission line profile, are fully cancelled. In order to carry out a proper subtraction, it is necessary that the spectra had comparable spectral resolutions. To obtain difference spectra, one usually subtracts either the mean spectrum or a spectrum representative of the minimum activity state.

Table 7. Year-averaged radial velocity of the blue and red bumps derived from the difference H β and H α profiles.

Year	H β radial velocity (km s $^{-1}$)			H α radial velocity (km s $^{-1}$)		
	V_b	V_{r1}	V_{r2}	V_{b1}	V_{r1}	V_{r2}
1996	-906 ± 131	$+1461 \pm 56$		-1200 ± 69	$+1379 \pm 103$	
1997	-833 ± 185	$+1216 \pm 164$		-696 ± 32	$+1079 \pm 64$	
1998	-994 ± 91	$+1137 \pm 103$		-1075 ± 67	$+1026 \pm 71$	
1999	-704 ± 200	$+838 \pm 155$		-944 ± 135	$+764 \pm 119$	
2000	-544 ± 134	+817:	$+2863 \pm 262$	-775 ± 192	+800:	$+2787 \pm 261$
2001	-704 ± 316	+954:	$+2707 \pm 70$	-1043 ± 172	+800:	$+2526 \pm 92$
2002	-938 ± 394	+674:	$+1898 \pm 200$	-1158 ± 144	+584:	$+1708 \pm 191$

We have adopted the second alternative, as the spectrum in the minimum state, provides us with crucial information about the contribution of the narrow emission and absorption lines, which are to be removed in order to carry a proper study of the profile shape changes with time. Hence, we obtained the H β and H α difference profiles by subtraction of the minimum activity state spectrum, represented by the mean spectrum of the May 15, 17 and June 4, 2002 observations for H β , and June 4, 2002 for H α . The subtraction was performed by our scaling program (see Appendix A), and a spectrum in minimum state was used as a reference. Since within every year, the shape of the line profiles changes only slightly, we have calculated the annual mean difference profiles for H β and H α (Fig. 8). Variations of the profiles similar to those on the observed H β and H α line profiles (see Sect. 3.2.3) are well seen. Peculiarities in the shape of the bumps in the difference profiles are better seen than on the observed profiles. In the H α difference profiles for 2000–2002, at radial velocity $\sim +1000$ km s $^{-1}$ a drop in brightness (dip) is seen, this is due to over-subtraction of the [NII] $\lambda 6584$ line. This is due to the fact that the *FWHM* of this line is smaller than the one for the [OIII] $\lambda 5007$ line, used to reduce the spectra to similar resolution (see Sect. 2.4). This effect becomes noticeably on the 2000–2002 spectra, when the flux in the broad components decreases by factors of the order of 2 to 3. From the monthly-averaged difference profiles of H β and H α , we defined the radial velocities of the peaks as the mean weighted location of the bump tops (for details see Sect. 3.2.3). Our results are listed in Table 7, there the annual averages for the radial velocities of the blue (V_b), and red (V_{r1} and V_{r2}) peaks along with their corresponding dispersion values are presented, for H β and H α . In Table 7, it is seen that the peak radial velocities of H β and H α for different years agree with each other within the errors. It may be noted that during 1996–1999, the radial velocities of the blue (V_b) and red bumps (V_{r1}) were, on average, close to ± 1000 km s $^{-1}$. However, it is distinctly seen that in 1996 the radial velocity of the red peak (V_{r1}) was larger than in subsequent years. During 2000–2001, a decrease of the radial velocity of the blue (V_b) peak in the H β difference profiles was observed. At that time the radial velocity determinations of the red peak (V_{r1}) from the difference profiles in 2001–2002 are uncertain (marked with a colon in Table 7), because in this velocity zone, a bending shoulder is present in the H β profile, and the previously mentioned dip in the

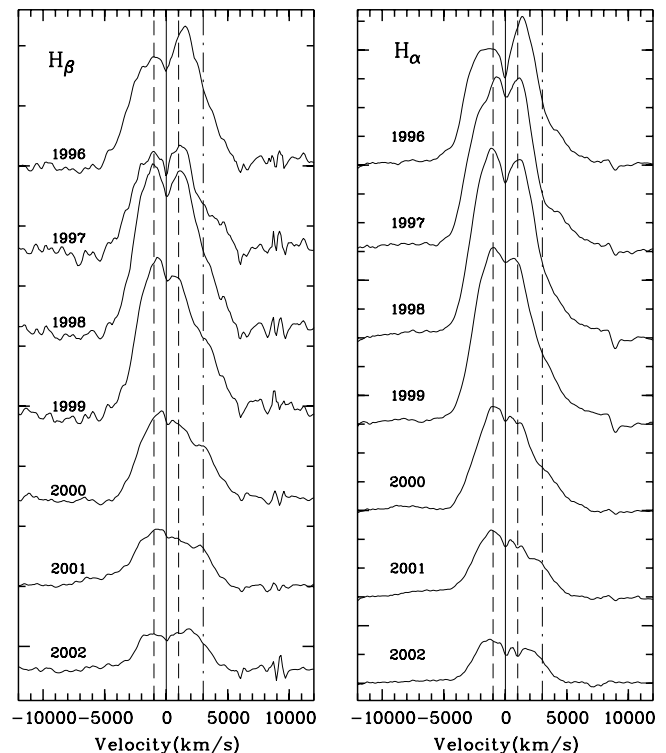


Fig. 8. Annual averages from 1996 to 2002 of the difference profiles of the broad H β (left panel) and H α (right panel) lines. The vertical lines correspond to the radial velocities: dashed lines: ± 1000 km s $^{-1}$; dash-dotted lines: $\sim +3000$ km s $^{-1}$; thin lines: 0 km s $^{-1}$. The abscissae represent the radial velocities relative to the narrow component of H β and H α . The ordinates give the relative fluxes. The profiles are shifted vertically by a constant value.

H α profile, due to over-subtraction of [NII] $\lambda 6584$, affects our results. In 2000 a new distinct red bump appeared with a radial velocity of about $+2800$ km s $^{-1}$ (V_{r2} in Table 7). By 2002 its radial velocity had decreased to about $+1800$ km s $^{-1}$, while its brightness became similar to that of the blue bump. We can definitely say that in the year 2000 a new bump in the red wing of the lines appeared and that its radial velocity decreased by about 1000 km s $^{-1}$ between 2000 and 2002.

3.3. Flux variability for different parts of H α and H β profiles

As mentioned above, the flux of the H β and H α emission lines as well as the $\lambda\lambda 5190$ continuum flux, varied significantly between 1996 and 2002. Some parameters of the variability were noted in Sect. 3.1. However, as it is shown in Sects. 3.2.3 and 3.2.4, important details such as bumps or oblique shoulders are present in the profiles of the broad lines. Therefore, it is of great interest to study the behaviour in time of these parts of the profiles relative to each other, and with respect to continuum variations. To this purpose, we have divided the emission line profiles into several radial velocity bins and constructed the data sets for a number of time series that are of interest. We have chosen symmetrical bins relative to zero radial velocity of the H β and H α line profiles. These bins include either distinct peaks or notable features that were observed at different times (see Sects. 3.2.3 and 3.2.4): the H β 1, H α 1 set from -3000 km s $^{-1}$ to -2000 km s $^{-1}$; the H β 2, H α 2 set from -1500 km s $^{-1}$ to -500 km s $^{-1}$; the H β 3, H α 3 set from $+500$ km s $^{-1}$ to $+1500$ km s $^{-1}$; the H β 4, H α 4 set from $+2000$ km s $^{-1}$ to $+3000$ km s $^{-1}$. The flux associated to those radial velocity bins are named as: Flux1, Flux2, Flux3, Flux4, respectively. Their light curves for H β and H α are plotted in Figs. 9 and 10 (left).

The upper left and right panels present the light curves for the continuum near H β (Fig. 9) and H α (Fig. 10). From these figures, one can see that the flux in different parts of H β and H α change in an almost identical manner.

3.3.1. The shapes of the H α and H β in relation to their variability

The broad H β and H α emission lines show changes in both: flux and shape of the profiles. Wanders & Peterson (1996) suggested a method for studying the variations of the profile shape by means of a normalization of the emission lines by their total flux and then see how these normalized profiles change in the course of time. They named shape the function $Fq(v, t)$, defined as:

$$Fq(v, t) = F(v, t) - [\langle F(v, t) \rangle / \langle F(t) \rangle] \cdot F(t), \quad (5)$$

where $F(v, t)$ is the flux in the profile at a radial velocity v at a time t ; $\langle F(v, t) \rangle$ and $\langle F(t) \rangle$ are the time-averaged (over the whole set of observations) flux at a radial velocity v and the total flux in the line, respectively; $F(t)$ is the total flux in the emission line at a time t . By definition one gets $\int Fq(v, t) dv = 0$, if the integration is performed over the whole emission line. The shape value in a given radial velocity interval (or the shape value in a given profile part) is defined by integrating Eq. (5) in this velocity interval. From Eq. (5), it follows that the value of $Fq(v, t)$ will be close to zero when the profile part $F(v, t)$ changes proportionally to the total flux $F(t)$. If the proportionality is violated due to delay effects or to some other reason, then $Fq(v, t)$ will be either positive or negative. A positive value $Fq(v, t)$ means that at a time t the given profile part is more prominent than in the average profile, while a negative value means that this part is less prominent. So, $F(v, t)$ is a

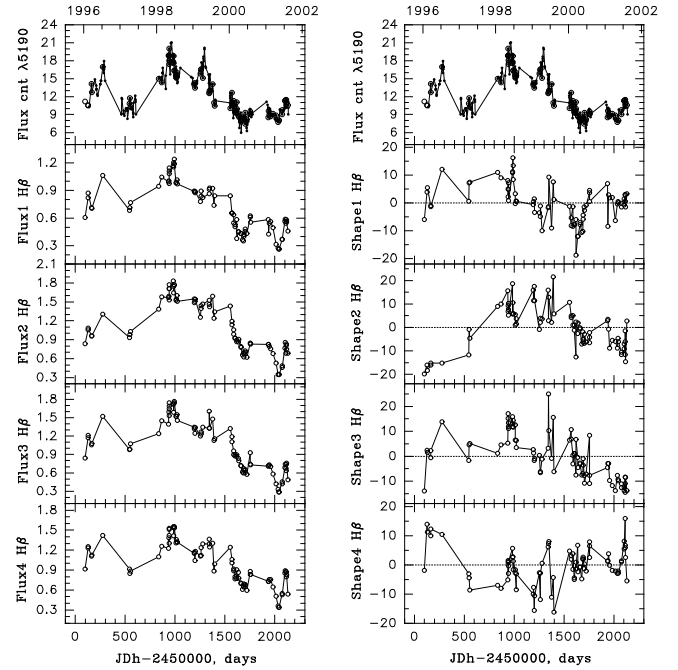


Fig. 9. Variations of the flux (left panel) and shapes (right panel) in different parts of the H β profile, and in the “combined” continuum at the observed wavelength $\lambda 5190$ Å. The radial velocity intervals of the profile segments: the H β 1, H α 1 set goes from -3000 km s $^{-1}$ to -2000 km s $^{-1}$; the H β 2, H α 2 set goes from -1500 km s $^{-1}$ to -500 km s $^{-1}$; the H β 3, H α 3 set goes from $+500$ km s $^{-1}$ to $+1500$ km s $^{-1}$; the H β 4, H α 4 set goes from $+2000$ km s $^{-1}$ to $+3000$ km s $^{-1}$. The flux in the lines are given in units of 10^{-13} erg cm $^{-2}$ s $^{-1}$, and in the continuum are given in units of 10^{-15} erg cm $^{-2}$ s $^{-1}$ Å $^{-1}$. The shapes are in relative units (see Sect. 3.3.1).

sensitive indicator of the relative prominence of a part of the profile. If the profile shapes vary due to reverberation effects, $Fq(v, t)$ must be correlated with the flux variations of the continuum after some delay.

We have considered four shape time series in the radial velocity intervals mentioned in Sect. 3.3: shape1 for $(-3000, -2000)$ km s $^{-1}$; shape2 for $(-1500, -500)$ km s $^{-1}$; shape3 for $(+500, +1500)$ km s $^{-1}$ and shape4 for $(+2000, +3000)$ km s $^{-1}$.

The changes of the shape of the different profile parts are shown on the right panels of Figs. 9 and 10, for H β and H α , respectively. The changes in shape behave differently from continuum variations: sometimes they change following the continuum changes, and some other time in quite the opposite manner. The behavior of the shape of different parts of the lines differs, though the changes of a given shape for H α and H β are similar.

3.3.2. The relations flux-shape and shape-continuum for the different parts of the H β and H α broad emission lines

A clear-cut distinction in the behavior of the flux and the shapes can be seen in Fig. 11, where we show the flux-flux,

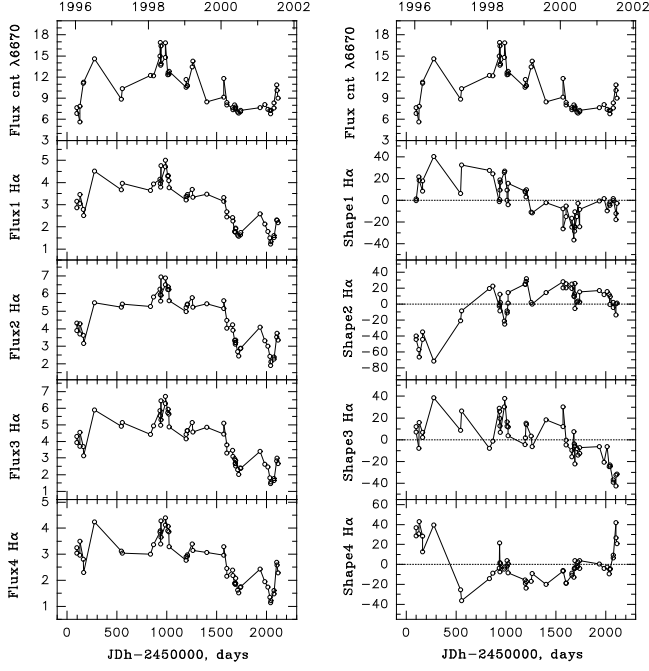


Fig. 10. Same as Fig. 9, but for $H\alpha$ and for the continuum at $\lambda 6670$.

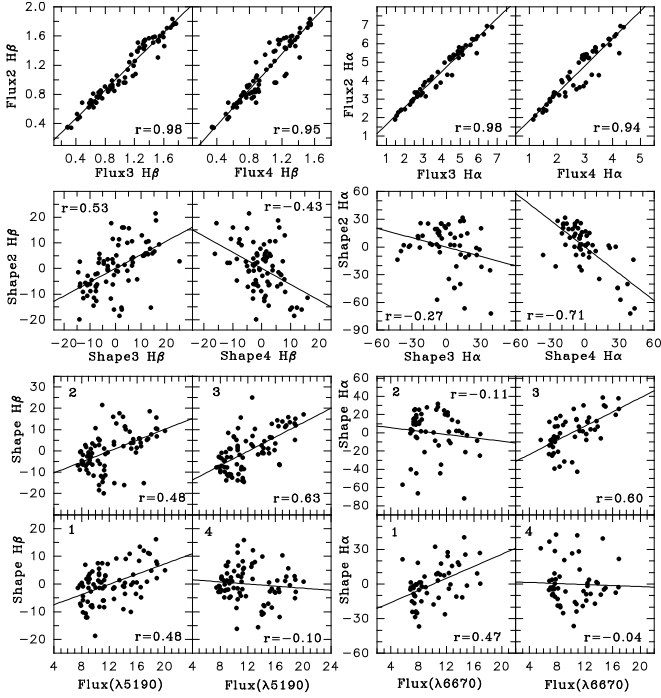


Fig. 11. Flux-flux, shape-shape and continuum flux-shape correlations for different parts of the $H\alpha$ and the $H\beta$ lines (the number shape is inside the plot). The correlation coefficients r are given inside the plot.

shape-shape and shape-continuum flux correlations for the different parts of the emission profiles of $H\beta$ and $H\alpha$.

There is a high degree of correlation between the flux in the various parts of $H\beta$ and $H\alpha$ (Fig. 11, top). The correlation coefficient values being 0.94–0.98. Yet, the correlations for the shapes of various parts of the lines are quite different. For example,

- the shape4 and shape2 have a tendency to be anti-correlated with each other;
- shape4 in $H\beta$ and $H\alpha$, including the bump at radial velocity $+2500 \text{ km s}^{-1}$, does not correlate with the continuum;
- shape2 in $H\beta$ is weakly related to the continuum, but the shape2 in $H\alpha$ is not;
- shape3 and shape2 have a tendency to be correlated in $H\beta$ and weakly anti-correlated in $H\alpha$;
- a good correlation with the continuum for the shape3 in $H\beta$ and $H\alpha$ is observed.

Note that the analysis of shape2 and shape3 in $H\alpha$, should be done with care, because the narrow components of $H\alpha$ and nitrogen are not properly subtracted in some profiles. Hence, the derived fluxes are subject to uncertainties, and the profiles in these regions may be considerably distorted. In the $H\beta$ case, the narrow component is well subtracted and data are more reliable. Therefore, from the $H\beta$ analysis alone, for shape2 and shape3 that include the double-peaks at radial velocities close to $\pm 1000 \text{ km s}^{-1}$, we conclude that they are weakly correlated with each other and also with the continuum.

Thus, the shape of the individual parts of the line profiles changes, unlike their fluxes, in a more complicated way. So, since the changes in shapes correlate sometimes slightly with the continuum changes, or do not correlation with them, then the changes may not be related to reverberation effects, and some other mechanisms should be invoked for their explanation.

3.4. The Balmer decrement

3.4.1. Integral Balmer decrement

From the spectra with the subtracted narrow component template (see Sect. 2.4), we determined the fluxes of $H\alpha$ and $H\beta$ emission line broad components within the radial velocity intervals $\pm 6000 \text{ km s}^{-1}$. The integral Balmer decrement (BD) is the flux ratio $F(H\alpha)/F(H\beta)$. Note that the FeII (42 multiplet) line at the rest wavelength 4924 \AA corresponds to a radial velocity of $+3874 \text{ km s}^{-1}$ relative to the narrow component of $H\beta$. This line sets in the broad red wing of $H\beta$ close to the blue wing of the emission line [OIII] 4959. No measurable feature is seen on our spectra at this place. Since it is known that the intensities of FeII 42 ($4924, 5018, 5169$) lines are comparable, we have estimated the contribution of FeII 42 5169 \AA line. This line is well seen on our spectra. We have obtained for the ratio of FeII 42 (5169) to the flux integrated within the interval of radial velocities $\pm 6000 \text{ km s}^{-1}$ (i.e. onto the broad component of $H\beta$): $F(\text{FeII } 42)/F(H\beta) \sim (0.02-0.03)$ in 1996–1999, and $\sim (0.03-0.06)$ in 2000–2001. Thus, the contribution of FeII 42 to the $H\beta$ broad component is $\sim (2-3)\%$ in 1996–1999, and $\sim (3-6)\%$ in 2000–2001. This is within the measurement errors of the Balmer decrement. Therefore, we did not take into account the contribution of FeII 42. Figure 12 shows the behavior of Balmer decrement (upper panel), the $\lambda 5190$ continuum, (middle panel), and the relation between changes of the Balmer decrement and continuum flux (bottom panel). There an anticorrelation between the changes of the Balmer

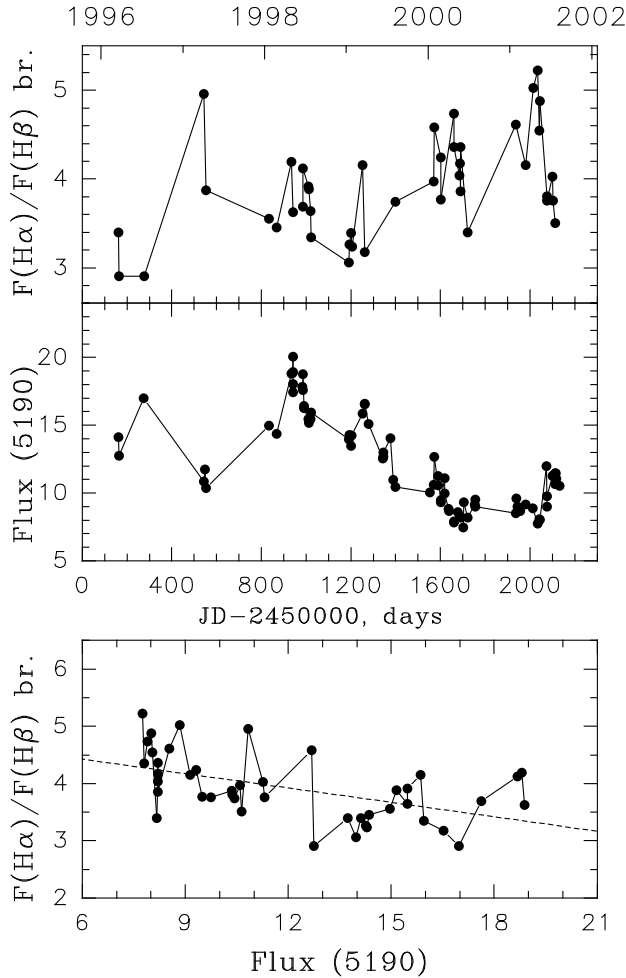


Fig. 12. Variations of the Balmer decrement $F(H\alpha)/F(H\beta)$ (top) and of the continuum flux (middle) in 1996–2001; variations of the Balmer decrement versus those of the continuum flux (bottom).

Table 8. The annual averaged Balmer decrement and continuum fluxes $F(\text{cont})$ at the observed wavelength $\lambda 5190 \text{ \AA}$.

Year	$F(H\alpha)/F(H\beta)$	$F(\text{cont})^*$
1996	3.48 ± 0.45	14.62 ± 2.2
1998	3.51 ± 0.44	16.96 ± 1.69
1999	3.51 ± 0.44	14.05 ± 1.62
2000	4.22 ± 0.42	9.27 ± 1.28
2001	4.33 ± 0.58	9.66 ± 1.26

* $F(\text{cont})$ in units of $10^{-15} \text{ (erg cm}^{-2} \text{ s}^{-1} \text{ \AA}^{-1}\text{)}$.

decrement and the continuum flux is evident (correlation coefficient ~ 0.52 , bottom panel in Fig. 12).

The same tendency is present in the annual averaged values of the BD and the continuum fluxes. In Table 8, the mean values of the Balmer decrement are listed for several years together with the mean values of the continuum flux.

From Table 8 it is seen that during 1996–1999 the average flux in the continuum varied slightly, while the Balmer decrement did not change. However, in 2000–2001 the average flux

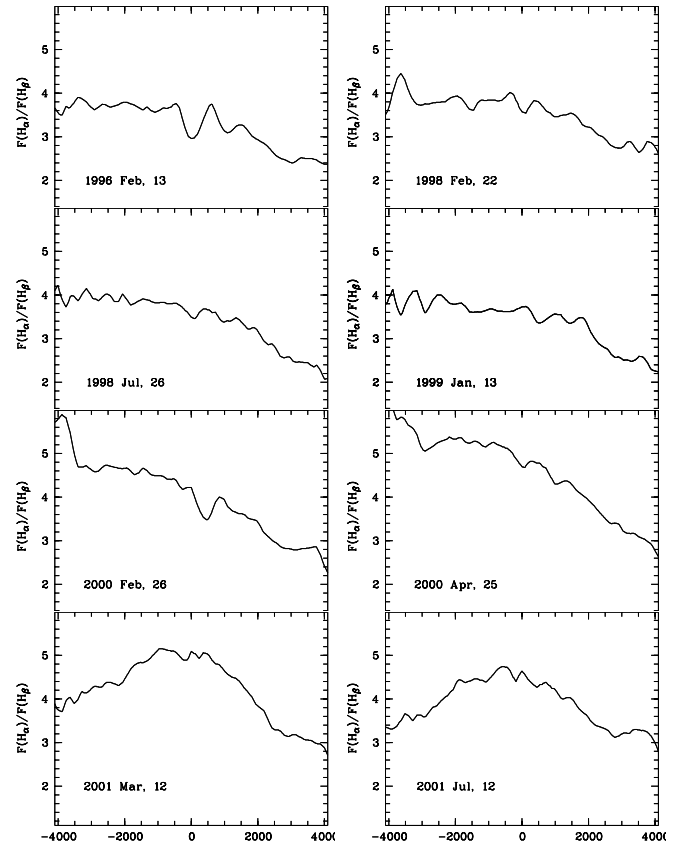


Fig. 13. Variations of the Balmer decrement $F(H\alpha)/F(H\beta)$ along some individual profiles of the broad lines. The abscissae represents the radial velocities relative to the narrow components.

in the continuum decreased and the Balmer decrement became considerably larger (steeper).

3.4.2. Balmer decrement across some individual profiles

Figure 13 shows the Balmer decrement across some individual broad lines profiles. The decrement is similar to that of other profiles for the same years. Yet, the Balmer decrement across the line profile changes from year to year. During 1996–1999 in the radial velocity interval from $\sim -4000 \text{ km s}^{-1}$ to $\sim +2000 \text{ km s}^{-1}$, the Balmer decrement varied only slightly and had a value of ~ 4.0 , while in the radial velocity interval $+ (2000-4000) \text{ km s}^{-1}$, it decreased, from ~ 4.0 to 2.0 . In the year 2000, the Balmer decrement increased, as a whole. Yet, a monotonic decrease with radial velocity is clearly present. During 2001, maximum values (~ 5) were observed at the line center, and at the edges the BD decreases with a somewhat larger gradient in the red wing.

4. Summary of our main results and comparison with other results from the literature

1. In Sect. 3.2 we have shown that the observed mean and rms profiles as well as the annual averaged, observed and difference profiles of H α and H β present a double-peak structure,

i.e. bumps at radial velocities $\sim\pm 1000$ km s $^{-1}$ (zero velocity being defined as that of the narrow components). While the double peaks were obtained after subtraction of the narrow line components, a question arises about the reality of these features, as it dependent on the method of subtraction of those components. The following facts are taken as evidence to the reality of the double peaks: 1) double-peaks are obtained on the variable component when the original H β and H α profiles are decomposed, before subtraction of the narrow components (Sect. 3.2.1); 2) the appearance of double peaks on the difference profiles of H β and H α , when the narrow lines are subtracted automatically (Sect. 3.2.4). The relative intensity of these peaks varied: in 1996, the red peak was brighter than the blue one, and viceversa, in 1998–2002, the blue peak became brighter. We have seen that the radial velocities of the double peak vary within $\sim\pm(500\text{--}1200)$ km s $^{-1}$.

The double-peaked structure in the central part of the broad lines in the radial velocity range $\sim\pm 500\text{--}1500$ km s $^{-1}$ was observed earlier. Double-peaks at velocities $\sim\pm 500$ km s $^{-1}$ were seen in the annual averaged profiles of H β in 1986–1987 by Wanders & Peterson (1996). On the individual difference profiles of H β , the double peaks were also evident in 1992 (Iijima & Rafanelli 1995). Very distinct double peaks were also noticeable on the difference H α profiles in July 1986–June 1985 (Stirpe et al. 1988) and in May 1987–July 1986 (Stirpe & de Bruyn 1991).

2. During 2000–2002, when the flux of the continuum and the lines greatly decreased, a new distinct peak at a radial velocity of $\sim+2500$ km s $^{-1}$ appeared on the profiles of H α and H β . This peak had comparable brightness to the blue peak at a radial velocity of $\lesssim-1000$ km s $^{-1}$ (Sect. 3.2.3). A radial velocity decrease of ~ 500 km s $^{-1}$ for this feature occurred between 2000 and 2002 (Table 6 and Fig. 7). The same peak is seen on the difference profiles of H α and H β (Sect. 3.2.4). Its radial velocity decreased as well, but by a larger value (~ 1000 km s $^{-1}$) than the one derived from the observed profiles. This is a result of the details present in the line profiles at minimum activity state, which are subtracted from the observed profiles. In the red wing of H β at minimum activity state, a distinct wide asymmetric weak bump is observed at a radial velocity of about $+2200$ km s $^{-1}$. Therefore on the difference profiles in the red wing, we observe excess emission relative to this weak bump in the spectrum at minimum state. Thus, from our data set, we can establish the appearance of a new peak in the red wings of H α and H β during 2000–2002. The radial velocity of this peak in 2002 decreased by $\sim 500\text{--}1000$ km s $^{-1}$, with respect to the value determined for the year 2000.
3. From the decomposition of H α and H β profiles (see Sect. 3.2.1) we have found that the fluxes of the variable component of the lines correlate well with the flux variations of the continuum. In the radial velocity interval ~-4000 km s $^{-1}$ to $\sim+5000$ km s $^{-1}$ the correlation coefficient has a high value $r \sim 0.8\text{--}0.9$. In Sect. 3.3, we have shown that the flux of different parts of the profiles, change in an almost identical manner being highly correlated both

with each other ($r \sim 0.94\text{--}0.98$) and with the continuum flux levels ($r \sim 0.88\text{--}0.97$). These facts indicate that the flux variability in different parts of the line profiles on short time scales is caused mainly by the reverberation effect.

4. Line profile shapes evolve slowly, on time scales of months to years. The shape variations of the different parts of the line profiles, mildly correlate with each other and/or with the continuum variations, or simply do not correlate at all (see Sect. 3.3.2 and Fig. 11). So, the profile shape changes on long time scales are not due to reverberation, as earlier discussed by Wanders & Peterson (1996).
5. The flux ratio of $F(\text{H}\alpha)/F(\text{H}\beta)$ (BD) shows a clear anti-correlation with the continuum flux (see Fig. 12 and Table 8). Such an effect has also been observed in other monitoring campaigns of Sy galaxies (Dietrich et al. 1993; Shuder 1981). In addition, there are changes of the Balmer decrement across the profiles and it varies from year to year (see Fig. 13).

5. Discussion

The study of the H α and H β broad line profiles in NGC 5548 with different techniques, shows the presence of double-peak structures at radial velocities $\sim\pm 1000$ km s $^{-1}$ relative to the narrow steady component (Sect. 4, point 1).

The appearance of double peaked structures in the profiles of broad emission lines is predicted by some types of models: a) different versions of accretion-disc models (Dumont & Collin-Souffrin 1990a,b; Rokaki et al. 1992; Chen & Halpern 1989; Eracleous et al. 1995); b) bi-conic gas flows (Veilleux & Zeng 1991); c) binary black holes (Gaskell 1983).

The strongest argument against the binary black hole model is the fact that the velocity curve of the H α red peak in 3C 390.3 (the most prominent object with double peaks) is inconsistent with the best-fitting binary models (Eracleous et al. 1997). Within the framework of the model of binary black hole, the appearance of the third peak in NGC 5548 at a radial velocity of $\sim+2500$ km s $^{-1}$ is impossible to explain. The biconical gas flows imply mainly radial motions in BLR, not supported by any observations. For instance, from the CCF analysis of the H β emission line profiles from the data of AGN-Watch monitoring in 1989–1993, Wanders & Peterson (1996) excluded the possibility of large radial motions in BLR of NGC 5548. Kollatschny & Dietrich (1996) showed that the outer wings of the Balmer lines have a tendency to repond faster than their cores to the continuum variations. We also tried to carry out the CCF analysis for different parts of the H α and H β profiles using our data. But because of our poor sample there were large uncertainties in the time delay determination. However, in spite of this, we noted that H α and H β show a same tendency for smaller time delays at high velocities than at low velocities, and that there is no time delay between the blue and red wings of H β within 3–4 days. Of course, our results are only qualitative, but they do not contradict the results of the AGN-Watch monitoring. Thus, the available observations indicate predominantly rotational (or virial) motions of NGC 5548 in BLR, and support the scenario of formation of the broad emission lines in an accretion disk. Assuming a standard geometrically thin

disc, Dumont & Collin-Souffrin (1990a,b) have shown that the broad Balmer lines can be almost entirely due to disc emission. They obtained a large variety of profiles, including double peak symmetrical profiles for non-relativistic cases. Relativistic corrections introduce profile asymmetries: the blue side of the profile becomes brighter than the red one. However, in 1996, the red peak was brighter than the blue one, while at other times (1998–2002), the blue peak was the brighter one. The cases when the red peak is brighter than the blue one, are in contradiction with the predictions of relativistic circular disc models. However, as the calculations of Eracleous et al. (1995) show, such case is possible, when the broad lines originate in a relativistic, eccentric disc. In this case the changes in the line profile shapes, will be mainly due to precession of the disc. If this is the case, the radial velocities and the intensities of the double peaks would change slowly (in timescales of months to years), without following the effects of reverberation.

An alternative explanation for the observed intensity variations of the double peaks relative to each other, is to involve local disc inhomogeneities, which may be responsible for some of the substructures of the emission line profiles. Actually it is now clear that at the BLR distance, the disc becomes gravitationally unstable (Collin & Huré 1999). At that point the disc is expected to be highly inhomogeneous, including clouds and possibly spiral arms and it is certainly not constituted by a uniform density medium (e.g. Bunk et al. 1990; Chakrabarti & Wiita 1994).

Another issue which must be taken into consideration, is the fact that the line emitting regions should be illuminated by the central continuum source, in order to be able to reprocess an important fraction of such radiation. It is now well established that the UV-X source has small dimensions as compared to the BLR (say $10\text{--}100R_G$, where R_G is the gravitational radius, the BLR being located at $10^{3-4}R_G$). So, if the BLR constitutes itself the outskirts of the disc, it should be *able to see* the central source. There to this aim, there are several possibilities:

- as suggested by Dumont & Collin (1990a,b), the central radiation can be back-scattered towards the disc, as most of the hard radiation is emitted in the soft X-ray range ($\ll 10$ keV). Yet, this requires a highly ionized Thomson thick medium, surrounding the disc and the central source. This medium would create a low energy cut-off (at many keV), which is not observed in the high energy spectrum of AGNs and would change dramatically the hard X-range spectrum due to multiple Compton scattering;
- the disc should extend vertically, up to a scale height equal to at least one tenth of the radius. This would imply that a good fraction of the observed velocity (tens of percent) shall be non-rotational in origin. Probably due to large scale chaotic gas dynamical motions – macro-turbulence – added on top of regular rotation;
- the disc can be geometrically thin but warped, as suggested by recent observations (Kinney et al. 2000). The warping could be due to self-irradiation instabilities (Pringle 1996), to misalignment of the spin of the BH with the disc (Bardeen & Peterson 1975), or to disc feeding through a misaligned inflow.

In 2000–2002, we detected a new peak at a radial velocity of $\sim +2500$ km s⁻¹ in the red wing of $H\alpha$ and $H\beta$. This bump moved gradually along the line profile and its radial velocity decreased between 2000 and 2002 by ~ 500 km s⁻¹ on the observed profiles and by ~ 1000 km s⁻¹ on the differential profiles (Sect. 4). On the normalized $H\beta$ profiles (1989–1993), Wanders & Peterson (1996) noted the periodical appearance of broad red- and blue-wing shoulders at radial velocities of $\sim \pm 2500$ km s⁻¹. According to these authors, their relative intensities change over the years, but not their positions in the line profile. They interpreted this fact with a model of cloud illumination by an anisotropic source. However, on the normalized $H\beta$ profiles shown by these authors, no distinct peaks (bumps) are noted. It looks more as an asymmetry in the line profiles, i.e. a brightness increase within the velocity interval $\pm 1000\text{--}2500$ km s⁻¹. It was impossible to determine the location of the peaks from these profiles, since they were absent. Possibly, during the period of 1989–1993, the components appearing periodically in the velocity interval $\pm(1000\text{--}2500)$ km s⁻¹ were very broad and of low contrast. Therefore, the averaged profile obtained after summation of a large amount of spectra, showed the brightness increase in the form of inclined shoulders. Note that in 1991–1993 Sergeev et al. (1994) observed a distinct low contrast broad emission feature in the far red wing of the $H\alpha$ profile. The radial velocity of this feature decreased from $\sim +4500$ km s⁻¹ in 1991 to $\sim +2100$ km s⁻¹ in 1993. So, from our observations and those of Sergeev et al. (1994), we deduce that the position of the bump changes with time in the line profile, and therefore the interpretation of Wanders & Peterson (1996) based on a constant radial velocity of the bump is not correct. We think that the appearance of such details (bumps) moving along the profile is due to inhomogeneities in the disk. For time scales of years, which correspond to the dynamical time of the BLR, one can invoke to account for these inhomogeneities, a structure like a spiral wave at ~ 10 light days from the center which would rotate at approximately the same speed as the disc, causing a shift of the peak in the profile in from 1000 to 2500 km s⁻¹ in a few years (for a black hole mass of 7×10^7 Mo, the rotation timescale is on the order of 20 years). Such a single spiral arm is also invoked to explain the profiles and their variations in the LINER/Seyfert 1 galaxy NGC 1097 (Storchi-Bergman et al. 2003). A spiral wave will make a “bump” in the disc, as it thicker than the rest of the disc. Therefore it would be more illuminated than the rest of the disc, causing a localized enhancement in the line profile. The rotation of the spiral wave should be accompanied by a change of the time lag between the continuum and the lines. In this case there is no obvious link between a decrease of the continuum flux level and a velocity shift of the bump.

There are however, other possible explanations different from that of a spiral arm. For instance one can invoke a hot spot due to a collision of the disc with a passing star (e.g. Syer et al. 1991; Chakrabarti & Wiita 1993), or the explosion of a supernova releasing a remnant (a “SN cloud”) (Collin & Zahn 1999). In this case, the emitting material should be receding, with a velocity increasing with time. In the model of the SN cloud, one can explain the correlated decrease of the continuum by

assuming that as the SN cloud grows, it begins to cover the line of sight of the central source (in such a dense environment, a supernova would be denser, with a much larger column density than a normal supernova, during a few years). In both cases the new material will be incorporated later on to the inner disc and the accretion rate will increase. But this would take place a long time after the explosion of the supernova or the capture of the star by the disc, in the viscous timescale of the inner disc, i.e. in tens of years, so we cannot check this hypothesis at present.

For the two peak structure, one could invoke a double-armed spiral shock structure as proposed by Chakrabarti & Wiita (1994).

In a detailed physical study of the Balmer line emitting region in NGC 5548, Dumont et al. (1998) considered a sample of observations spanning a relatively small time (9 months) in 1989. They concluded that it must be heated partially by a non radiative mechanism, in particular because the variations of the lines were too small compared to those of the UV continuum in short term scales. Indeed, we noticed in the present paper that the line flux variations are very small in short time scales. This non radiative heating can be due for instance to sound waves. Such waves can be easily provided by a spiral wave or by a supernova, or by a star colliding with the disc.

So, we can suggest that the BLR is a highly turbulent medium in rotation constituting a kind of semi-thick inhomogeneous disc. It is partly heated by the central UV-X source, and partly mechanically through the dissipation of turbulent motions. At short time scales, instabilities of the inner disc create rapid changes of the continuum flux, inducing the reverberation effects, but smoothed by the non radiative part of the heating which varies much more slowly. At longer time scales, structural changes of the BLR induce changes of the line profiles and of the reverberated flux, and should lead after some years to changes in the accretion rate and consequently changes in the continuum flux. The inhomogeneities in the disc will boost the emissivity at specific radial velocities, thus producing bumps or asymmetries in the line profiles. However, one cannot choose among a variety of models of inhomogeneous disc the one which suits better the observed evolution of the Balmer line profiles in NGC 5548 in 1996–2002.

The variations of the integral Balmer decrement can also be interpreted in this framework. In Sect. 4 (point 5), we pointed out that the integrated Balmer decrement is anticorrelated with the continuum flux level. As the line flux in H α and H β correlates well with that of the continuum, we infer that the change of the integrated Balmer decrement is also caused by changes in the continuum flux. Indeed, when the ionization parameter decreases for a constant density plasma, an increase of $F(\text{H}\alpha)/F(\text{H}\beta)$ intensity ratio is expected (cf. for instance Wills et al. 1985). This is due to the decrease of the excitation state of the ionized gas: the temperature of the ionized zone being smaller, the population of the upper levels with respect to the lower ones decreases. However the great differences observed in the behaviour of the Balmer decrement along the individual profiles are certainly not due to the variations of the ionizing flux, as they take place in longer time scales. They are more probably due to local density fluctuations of the inhomogeneous medium, leading also to variations of the

ionization parameter, and inducing changes of the Balmer decrement across the line profiles.

6. Conclusions

Between 1996 and 2002, we have carried out a spectral monitoring of the Seyfert galaxy NGC 5548. It is found that the flux in the lines and the continuum gradually decreased and reached minimum values in May–June 2002, i.e. the continuum source gradually faded. The line wings at maximum light states (1998) correspond to a Sy1 type, while at minimum light states (2002), they are similar to a Sy1.8 type. It was shown that the observed mean and rms line profiles, the variable part of the H β and H α profiles, and the difference profiles present double peaks at radial velocities $\sim\pm 1000 \text{ km s}^{-1}$. During 1996, the red peak was brighter than the blue one, and in other years (1998–2002) the blue peak became brighter than the red one. In 2000–2002, we observed a third distinct peak in the red wings of H α and H β , at a radial velocity of $\sim+2500 \text{ km s}^{-1}$. The radial velocity of this peak decreased from 2000 to 2002 by $\sim 500 \text{ km s}^{-1}$ on the observed profiles, i.e. this peak moved gradually across the line profile towards lower radial velocities. The observed fluxes in different parts of the broad lines vary quasi-simultaneously. The flux in different parts of the profiles, are well correlated with each other, and with the continuum flux as well. Yet, the change in shapes of the various parts of the lines, either they weakly correlate, or simply do not correlate at all with the changes in the continuum flux. Hence, these changes are not caused by reverberation effects. We have observed a general increase of the integral Balmer decrement with a continuum flux decrease. This probably due to a decrement in the ionization parameter, caused by a decrease of the flux in the continuum. The behavior of the Balmer decrement across the line profiles, differs greatly from time to time, is probably due to variations of density in inhomogeneities in an accretion disc.

Section 5 tries to integrate all these observations in the framework of a model, and presents arguments in favor of the formation of the broad Balmer lines in a turbulent, partly mechanically heated accretion disc including large, moving “thick” inhomogeneities, capable of reprocessing the central source continuum.

Acknowledgements. The authors are grateful to Gaskell C. M. and Komberg B. V. for useful discussions, Sergeev S. G. for providing a number of service programs, Spangenberg L. I. for help in preparing the paper, and Zhdanova V. E. for help in processing the spectra. This paper has had financial support from INTAS (grant N96-0328), RFBR (grants N97-02-17625, N00-02-16272 and N03-02-17123), state program “Astronomy” (Russia), and CONACYT research grants G28586-E, 32106-E, and 39560-F (Mexico).

References

- Antokhin, I. I., & Bochkarev, N. G. 1983, AZh, 60, 448
- Bahcall, J. N., Kozlovsky, B., & Salpeter, E. E. 1972, ApJ, 171, 467
- Bardeen, J. M., & Petterson, J. A. 1975, ApJ, 195, L65
- Bunk, W., Livio, M., & Verbunt, F. 1990, A&A, 232, 371
- Begelman, M. C. 1985, in *Astrophysics of Active Galaxies and Quasi-Stellar Objects*, ed. J. S. Miller (Mill Valley, CA: Univ. Sci.), 411

- Blandford, R. D., & McKee, C. F. 1982, *ApJ*, 255, 419
- Bochkarev, N. G., & Antokhin, I. 1982, *Astron. Tsirk.*, 1238, 1
- Chakrabarti, S. K., & Wiita, P. 1993, *ApJ*, 411, 602
- Chakrabarti, S. K., & Wiita, P. 1994, *ApJ*, 434, 518
- Chen, K., & Halpern, J. P. 1989, *ApJ*, 344, 115
- Clavel, J., Reichert, G. A., Alloin, D., et al. 1991, *ApJ*, 366, 64
- Collin, S., & Huré, J.-M. 1999, *A&A*, 341, 385
- Collin, S., & Zahn, J.-P. 1999, *A&A*, 344, 433
- Crenshaw, D. M., & Blackwell, J. H. 1990, *ApJ*, 358, L37
- Dietrich, M., Kollatschny, W., Peterson, B. M., et al. 1993, *ApJ*, 408, 416
- Dietrich, M., Bender, C. F., Bergmann, D. J., et al. 2001, *A&A*, 371, 79
- Doroshenko, V. T., Lyuty, V. M., Bochkarev, N. G., et al. 2001, *Astron. Lett.*, 27, 691
- Dumont, A. M., & Collin-Souffrin, S. 1990a, *A&A*, 229, 302
- Dumont, A. M., & Collin-Souffrin, S. 1990b, *A&A*, 229, 313
- Dumont, A., Collin-Souffrin, S., & Nazarova, L. 1998, *A&A*, 331, 11
- Eracleous, M., Livio, M., Halpern, J. P., & Storchi-Bergmann, T. 1995, *ApJ*, 438, 610
- Eracleous, M., Halpern, J. P., Gilbert, A. M., Newman, J. A., & Filippenko, A. V. 1997, *ApJ*, 490, 216
- Gaskell, C. M. 1983, in *Quasars and Gravitational Lenses*, Proc. 24th Liège Astrophys. Coll. (Liege: Inst. d'Astrophys., Univ. Liège), 473
- Iijima, T., & Rafanelli, P. 1995, *A&AS*, 113, 493
- Kinney, A. L., Schmitt, H. R., Clarke, C. J., et al. 2000, *ApJ*, 537, 152
- Korista, K. T. 1994, *Reverberation Mapping of the Broad-Line Region in Active Galactic Nuclei*, ed. P. M. Gondhalekar, K. Horne, & B. M. Peterson, ASP Conf. Ser., 69, 185
- Korista, K. T., Alloin, D., Barr, P., et al. 1995, *ApJS*, 75, 719
- Kollatschny, W., & Dietrich, M. 1996, *A&A*, 314, 43
- Nelder, J. A., & Mead, R. 1965, *Comput. J.*, 7, 308
- Peterson, B. M. 1987, *ApJ*, 312, 79
- Peterson, B. M. 1993, *PASP*, 105, 247
- Peterson, B. M., Korista, K. T., & Cota, A. 1987, *ApJ*, 312, L1
- Peterson, B. M., Balonek, T. J., Barker, E. S., et al. 1991, *ApJ*, 368, 119
- Peterson, B. M., Berlind, P., Bertram, R., et al. 1994, *ApJ*, 425, 622
- Peterson, B. M., Pogge, R. W., Wanders, I., Smith, S. M., & Romanishin, W. 1995, *PASP*, 107, 579
- Peterson, B. M., Barth, A. J., Berlind, P., et al. 1999, *ApJ*, 510, 659
- Peterson, B. M., Berlind, P., Bertram, R., et al. 2002, *ApJ*, 581, 197
- Pringle, J. E. 1996, *MNRAS*, 281, 357
- Rees, M. J. 1984, *ARA&A*, 22, 471
- Rokaki, E., Boisson, C., & Collin-Souffrin, S. 1992, *A&A*, 253, 57
- Rokaki, E., & Boisson, C. 1999, *MNRAS*, 307, 41
- Shapovalova, A. I., Bochkarev, N. G., Burenkov, A. N., et al. 2001a, *Astron. Astroph. Trans.*, 20, 361
- Shapovalova, A. I., Burenkov, A. N., Bochkarev, N. G., et al. 2001b, *Astron. Astroph. Trans.*, 20, 349
- Shapovalova, A. I., Burenkov, A. N., Borisov, N., et al. 2002, *Active Galactic Nuclei: From Central Engine to Host Galaxy*, ed. S. Collin, F. Combes, & I. Shlosman, ASP Conf. Ser., 290, 253
- Shuder, J. M. 1981, *AJ*, 86, 1595
- Sergeev, S. G., Malkov, Yu. F., Chuvaev, K. K., & Pronik, V. I. 1994, *Reverberation Mapping of the Broad-Line Region in Active Galactic Nuclei*, ed. P. M. Gondhalekar, K. Horne, & B. M. Peterson, ASP Conf. Ser., 69, 199
- Spiridonova, O. I. 2002, private communication
- Stirpe, G. M., de Bruyn, A. G., & van Groningen, E. 1988, *A&A*, 200, 9
- Stirpe, G. M., & de Bruyn, A. G. 1991, *A&A*, 245, 355
- Storchi-Bergman, T., Nemmen da Silva, R., Eracleous, M., et al. 2003, *ApJ*, 598, 956
- Syer, D., Clarke, C. J., & Rees, M. J. 1991, *MNRAS*, 250, 505
- Van Groningen, E., & Wanders, I. 1992, *PASP*, 104, 700
- Veilleux, S., & Zheng, W. 1991, *ApJ*, 377, 89
- Vlasyuk, V. V. 1993, *Bull. Spec. Astrophys. Obs.*, 36, 107
- Wandel, A., Peterson, B. M., & Malkan, M. A. 1999, *ApJ*, 526, 579
- Wanders, I., Goad, M. R., Korista, K. T., et al. 1995, *ApJ*, 453, L87
- Wanders, I., & Peterson, B. M. 1996, *ApJ*, 466, 174
- Wills, B. J., Netzer, H., & Wills, D. 1985, *ApJ*, 288, 94

Online Material

Appendix A: Modification of the spectrum scaling method

In the monitoring programs of AGN, the spectral scaling scheme described by van Groningen & Wanders (1992) is used. The main idea of the algorithm is the creation of the difference spectrum between an input spectrum and a reference spectrum, for which the flux is assumed to be constant. The difference spectrum is represented by the simple analytical function (usually by a 2nd order polynomial). Then a χ^2 of this correspondence is minimized by a grid search method by successive variations of 3 input parameters: a flux scaling factor, a wavelength shift, and a difference in resolution of the spectrum ($\Delta FWHM$). For the latter, a convolution with Gaussian function is selected. For data with the S/N ratio ~ 10 , the error of the flux scaling factor is $<5\%$. However, the method of van Groningen & Wanders (1992) is unstable to the selection of initial parameters (the zero approximation is done manually). In order to circumvent this problem, we have modified the method. The difference between the individual spectra (obj) and the “reference” one (ref) is represented by a 3rd degree polynomial, and for the minimization of the differences, a downhill simplex method by Nelder & Mead (1965) is used. The latter is more stable than the grid search method used by van Groningen & Wanders (1992). As a zero approximation, the flux in the spectrum lines was determined automatically after subtraction of a linear continuum determined by the beginning and the end of a given spectral interval. The scaling procedure is then carried out with the program means in IDL, the program is fast and stable. The program output is similar to that of van Groningen & Wanders (1992): the flux scaling factor, relative wavelength shift and Gaussian width which is used for convolution with one of the spectra for spectral resolution correction, values of χ^2 and σ for the power approximation to the spectrum difference, the scaled and difference spectra (obj-ref). The latter are obtained after reducing the spectra to the same spectral resolution. In order to check the correctness of the scaling method several tests have been carried out.

1. We have tested the accuracy in the determination of the flux scaling factor by means of a model spectrum of different S/N ratios. As model data, we adopted the result of a multi Gaussian approximation to the Jan. 21, 1998 NGC 5548

spectrum, for the wavelength interval (4700–5400) Å including the [O III] $\lambda\lambda$ 4959, 5007 and H β emission lines.

In testing, the oxygen line intensities remained constant while the H β intensity was varied between 10 and 500 percent (H β = 100% corresponded to the observed spectrum of NGC 5548 in Jan. 21 1998). A continuum level was added to the lines and the spectrum was convolved with grey noise, to a chosen value of the S/N ratio. 200 experiments were carried out for each of the selected S/N ratios. From the simulated spectra with $S/N = 20$, the average values of the flux scaling factor show systematic decrease from 1.015 to 0.995 for changes of the H β intensity from 10% to 500%. The dispersion of the flux scaling factor being about 2.5%. As the S/N ratio is increased to 40 (typical value for spectra obtained in our monitoring campaign), systematic errors and dispersion values went down to 0.5% and 1% respectively.

2. With the model spectra we tested the method accuracy for the determination of the flux scaling factor in the case in which spectra of different resolution are compared. In this case the model spectrum adopted is the same as in case 1., with H β intensity 100%, but before introducing noise, a convolution with a Gaussian of the proper width is done. The value of the Gaussian dispersion ($\sigma = FWHM/2.35$) varied from 0.01 to 5.59 pixels with steps of 0.01 pixel (dispersion being 2 Å/px). We found that for spectra with S/N ratio ~ 20 , the value of $\sigma \geq 0.51$ and the flux scaling factor varies by less than 1%. We also checked for changes of the flux scaling factor in the observed blue spectra of NGC 5548. For this purpose, we first scaled the spectra adopting a spectrum with a resolution (~ 8 Å) as a referenced one. Then, the scaled spectra were processed by the program adopting a spectrum of lower resolution (~ 15 Å) as a the reference one. The values for the flux scaling factors so derived, coincided within an accuracy of $\sim 1\%$.
3. The wavelength shift ($\Delta\lambda$) is always recovered with high accuracy by the method.

Thus by scaling our AGN spectra by means of the modified method of van Groningen & Wanders (1992) as described above, one can obtain correct values of the scale parameters, their errors being dependent only on the quality of the spectra.

Appendix B: The tables presented in electronic form**Table B.1.** Log of the spectroscopic observations. Columns: 1 – number; 2 – UT date; 3 – Julian date; 4 – code according to Table 1; 5 – projected spectrograph entrance apertures; 6 – wavelength range covered; 7 – spectral resolution; 8 – mean seeing; 9 – position angle (PA) in degrees; 10 – signal to noise ratio in the continuum (5160–5220) Å near H β and (6940–7040) Å near H α .

No	UT-date	JD (2 400 000+)	Code	Aperture (arcsec)	Sp. range (Å)	Res. (Å)	Seeing arcsec	PA (deg)	S/N 5160–5220 Å
1	2	3	4	5	6	7	8	9	10
1	1996 Jan. 14	50 097.570	L1	2.4 × 13.5	3600–7200	9	4		28
2	1996 Jan. 15	50 098.581	L1	4.2 × 13.5	3600–7200	9	4		17
3	1996 Feb. 14	50 127.579	L	1.5 × 6.0	3100–5800	6	2		95
4	1996 Feb. 14	50 127.569	L	1.5 × 6.0	4500–7200	6	2		69
5	1996 Feb. 14	50 128.432	L	1.5 × 6.0	3100–5700	6	3		114
6	1996 Feb. 14	50 128.472	L	1.5 × 6.0	4500–7200	6	2		138
7	1996 Mar. 19	50 162.382	L	2.0 × 6.0	3600–5600	8	3	40	83
8	1996 Mar. 19	50 162.399	L	2.0 × 6.0	4700–7400	6	3	40	92
9	1996 Mar. 21	50 164.395	L	2.0 × 6.0	3600–5600	8	3	45	79
10	1996 Mar. 21	50 164.412	L	2.0 × 6.0	4700–7400	6	3	45	77
11	1996 Jul. 10	50 275.283	L	2.0 × 6.0	3600–5400	8	1.4	82	96
12	1996 Jul. 10	50 275.353	L	2.0 × 6.0	5200–7000	8	1.4	82	114
13	1997 Apr. 05	50 544.414	L1	4.2 × 19.8	4100–5900	9	4	90	40
14	1997 Apr. 05	50 544.455	L1	4.2 × 19.8	5500–7300	9	4	90	29
15	1997 Apr. 08	50 547.331	L	2.0 × 6.0	4444–5244	4.5	3	6	30
16	1997 Apr. 14	50 553.322	L	2.0 × 6.0	4400–5300	4.5	4	9	41
17	1997 Apr. 14	50 553.330	L	2.0 × 6.0	6200–7100	4.5	4	9	44
18	1998 Jan. 21	50 834.632	L	2.0 × 6.0	3800–6200	8	3	62	97
19	1998 Jan. 21	50 834.639	L	2.0 × 6.0	5900–7598	8	3	69	126
20	1998 Feb. 23	50 867.535	L	2.0 × 6.0	3800–6200	8	2	53	73
21	1998 Feb. 23	50 867.539	L	2.0 × 6.0	5900–7598	8	2	58	94
22	1998 Apr. 27	50 931.474	L1	8.0 × 19.8	5500–7300	9	4		28
23	1998 Apr. 30	50 934.438	L1	8.0 × 19.8	5500–7300	9	4	146	48
24	1998 Apr. 30	50 934.467	L1	8.0 × 19.8	4000–5800	9	4	146	73
25	1998 May 04	50 938.293	L	2.0 × 6.0	3700–6200	8	2.5	22	63
26	1998 May 04	50 938.289	L	2.0 × 6.0	5900–7598	8	2.5	20	49
27	1998 May 06	50 940.433	L	2.0 × 6.0	3700–6200	8	3	108	62
28	1998 May 06	50 940.436	L	2.0 × 6.0	5900–7598	8	3	107	54
29	1998 May 07	50 941.551	L	2.0 × 6.0	3700–6200	8	3	93	106
30	1998 May 08	50 942.452	L	2.0 × 6.0	4100–5450	4.5	2	104	41
31	1998 May 08	50 942.461	L	2.0 × 6.0	3700–6200	8	2	102	78
32	1998 May 08	50 942.472	L	2.0 × 6.0	5700–7700	8	2	100	22
33	1998 Jun. 17	50 982.407	L1	8.0 × 19.8	4050–5850	9	2	0	74
34	1998 Jun. 19	50 984.287	L1	8.0 × 19.8	4050–6147	9	4	0	81
35	1998 Jun. 19	50 984.328	L1	8.0 × 19.8	5500–7300	9	4	0	47
36	1998 Jun. 20	50 985.350	L1	8.0 × 19.8	4050–6000	9	2	0	67
37	1998 Jun. 20	50 985.281	L1	8.0 × 19.8	5500–7300	9	2	0	32
38	1998 Jun. 25	50 990.409	L	2.0 × 6.0	3600–6100	8	3	84	61
39	1998 Jun. 26	50 991.331	L	2.0 × 6.0	3600–6100	8	2	102	40
40	1998 Jul. 14	51 008.778	GH	2.5 × 6.0	3979–7230	15	2	90	106
41	1998 Jul. 17	51 011.683	GH	2.5 × 6.0	4210–7471	15	2	90	84
42	1998 Jul. 26	51 020.703	GH	2.5 × 6.0	3960–7231	15	2.2	90	73
43	1998 Jul. 27	51 021.712	GH	2.5 × 6.0	3930–7219	15	2.5	90	85

Table B.1. continued.

No	UT-date	JD (2 400 000+)	Code	Aperture (arcsec)	Sp. range (Å)	Res. (Å)	Seeing arcsec	PA (deg)	S/N 5160–5220 Å
1	2	3	4	5	6	7	8	9	10
44	1999 Jan. 13	51 191.952	GH	2.5 × 6.0	4150–7436	15	2.4	90	94
45	1999 Jan. 14	51 193.011	GH	2.5 × 6.0	4151–7438	15	2	90	94
46	1999 Jan. 22	51 200.542	L1	4.2 × 19.8	4000–5800	9	3	90	62
47	1999 Jan. 23	51 201.579	L1	4.2 × 19.8	5550–7350	9	3	90	57
48	1999 Jan. 25	51 203.565	L1	4.2 × 19.8	4000–5800	9	4	90	49
49	1999 Jan. 26	51 204.576	L1	4.2 × 19.8	5550–7350	9	4	90	59
50	1999 Mar. 15	51 252.970	GH	2.5 × 6.0	4200–7500	15	2	90	138
51	1999 Mar. 24	51 262.444	L1	4.2 × 19.8	4050–5850	9	3	90	68
52	1999 Mar. 24	51 262.452	L1	4.2 × 19.8	5550–7350	9	3	90	15
53	1999 Mar. 24	51 262.452	L	2.0 × 6.0	4260–5520	4.5	3	89	93
54	1999 Apr. 11	51 279.533	L1	4.2 × 19.8	4050–5850	9	4	0	59
55	1999 Jun. 12	51 342.409	L1	4.2 × 19.8	3999–5796	9	3	0	29
56	1999 Jun. 14	51 344.354	L1	4.2 × 19.8	4050–5850	9	3	90	63
57	1999 Jun. 16	51 346.335	L1	4.2 × 19.8	4050–5850	9	3	90	21
58	1999 Jul. 16	51 376.277	L	2.0 × 6.0	4000–5840	8	2	138	72
59	1999 Jul. 30	51 390.253	L1	4.2 × 19.8	4000–5800	9	2	0	34
60	1999 Aug. 08	51 399.254	L1	4.2 × 19.8	4000–5800	9	4	0	41
61	1999 Aug. 09	51 400.245	L1	4.2 × 19.8	5550–7350	9	2	0	35
62	2000 Jan. 10	51 553.567	L1	4.2 × 19.8	4000–5800	9	3	90	78
63	2000 Jan. 27	51 570.959	GH	2.5 × 6.0	4070–7350	15	2.5	90	83
64	2000 Jan. 28	51 571.914	GH	2.5 × 6.0	4070–7350	15	1.5	90	72
65	2000 Feb. 14	51 588.510	L1	4.2 × 19.8	4020–5820	9	4	90	53
66	2000 Feb. 15	51 589.506	L1	4.2 × 19.8	4030–5830	9	4	90	73
67	2000 Feb. 26	51 600.898	GH	2.5 × 6.0	4560–7850	15	2.2	90	85
68	2000 Feb. 27	51 601.847	GH	2.5 × 6.0	4310–7600	15	2.5	90	97
69	2000 Mar. 14	51 618.483	L1	4.2 × 19.8	4050–5850	9	4	90	34
70	2000 Mar. 15	51 619.478	L1	4.2 × 19.8	4050–5850	9	4	90	50
71	2000 Apr. 01	51 636.414	L1	4.2 × 19.8	4100–5900	9	4	90	32
72	2000 Apr. 04	51 639.397	L1	4.2 × 19.8	4050–5850	9	3	90	41
73	2000 Apr. 25	51 659.839	GH	2.5 × 6.0	4210–7460	15	2.2	90	61
74	2000 Apr. 26	51 660.815	GH	2.5 × 6.0	4210–7460	15	2.2	90	48
75	2000 May 11	51 676.365	L1	4.2 × 19.8	4050–5850	9	3	90	48
76	2000 May 16	51 681.283	L1	4.2 × 19.8	5550–7350	9	3	90	52
77	2000 May 20	51 685.321	L1	4.2 × 19.8	5600–7400	9	2	90	61
78	2000 May 21	51 686.258	L1	4.2 × 19.8	4050–5850	9	3	90	53
79	2000 May 21	51 686.350	L1	4.2 × 19.8	5550–7350	9	2	90	41
80	2000 May 25	51 689.786	GH	2.5 × 6.0	4130–7400	15	2.5	90	96
81	2000 May 26	51 690.835	GH	2.5 × 6.0	4134–7380	15	2.5	90	71
82	2000 Jun. 06	51 702.378	L1	4.2 × 19.8	4020–5820	9	3	90	56
83	2000 Jun. 08	51 704.299	L1	4.2 × 19.8	4020–5820	9	3	90	47
84	2000 Jun. 15	51 711.308	L1	4.2 × 19.8	5600–7400	9	3	90	41
85	2000 Jun. 25	51 721.712	GH	2.5 × 6.0	4690–7980	15	2.8	90	49
86	2000 Jul. 12	51 738.335	L1	4.2 × 19.8	5560–7360	9	3	90	33
87	2000 Jul. 13	51 739.275	L1	4.2 × 19.8	5560–7360	9	3	90	44
88	2000 Jul. 28	51 754.269	L1	4.2 × 19.8	4060–5860	9	3	90	38
89	2000 Jul. 29	51 755.301	L1	4.2 × 19.8	4040–5840	9	2	90	46
90	2000 Jul. 30,31 ^a	51756.786	L1	4.2 × 19.8	4040–5840	9	2	90	90
91	2001 Jan. 25	51 935.482	L1	4.2 × 19.8	4050–5850	9	2	90	77
92	2001 Jan. 26	51 936.517	L1	4.2 × 19.8	5550–7350	9	2	90	58
93	2001 Jan. 29	51 938.560	L1	4.2 × 19.8	4094–5740	9	2	90	58

Table B.1. continued.

No	UT-date	JD (2400 000+)	Code	Aperture (arcsec)	Sp. range (Å)	Res. (Å)	Seeing arcsec	PA (deg)	S/N 5160–5220 Å
1	2	3	4	5	6	7	8	9	10
94	2001 Feb. 03	51 944.498	L1	4.2 × 19.8	4094–5740	9	2	90	54
95	2001 Feb. 16	51 957.492	L1	4.2 × 19.8	4094–5740	9	2	90	52
96	2001 Mar. 13	51 981.867	GH	2.5 × 6.0	4120–7390	15	2.5	90	78
97	2001 Apr. 13	52 013.360	L1	4.2 × 19.8	4094–5740	9	3	90	69
98	2001 Apr. 13	52 013.451	L1	4.2 × 19.8	5550–7350	9	3	90	50
99	2001 May 05	52 034.784	GH	2.5 × 6.0	4156–7460	15	2	90	113
100	2001 May 12	52 041.829	GH	2.5 × 6.0	3600–6900	15	1.8	90	96
101	2001 May 14	52 043.859	GH	2.5 × 6.0	3980–7300	15	1.8	90	125
102	2001 Jun. 14	52 074.772	GH	2.5 × 6.0	4022–7330	15	1.8	90	93
103	2001 Jun. 15	52 075.738	GH	2.5 × 6.0	4010–7330	15	1.8	90	100
104	2001 Jul. 10	52 101.367	L	2.0 × 6.0	3630–6050	8	2	90	56
105	2001 Jul. 10	52 101.367	L	2.0 × 6.0	5740–8050	8	2	90	25
106	2001 Jul. 12	52 103.283	L	2.0 × 6.0	3630–6050	8	2	0	107
107	2001 Jul. 12	52 103.283	L	2.0 × 6.0	5740–8050	8	2	0	63
108	2001 Jul. 21	52 112.340	L1	4.2 × 19.8	4042–5800	9	2	90	34
109	2001 Jul. 22	52 113.261	L	2.0 × 6.0	3600–6020	8	2	0	92
110	2001 Jul. 22	52 113.261	L	2.0 × 6.0	5740–8050	8	2	0	46
111	2001 Jul. 23	52 114.335	L1	8.0 × 19.8	4094–5746	9	2	90	47
112	2001 Jul. 26	52 117.333	L1	8.0 × 19.8	4094–5746	9	2	90	62
113	2001 Aug. 09	52 131.300	L1	4.2 × 19.8	4400–6200	9	2	90	40
114	2002 May 15	52 410.456	L1	4.2 × 19.8	4400–6200	9	2	90	52
115	2002 May 17	52 412.435	L1	4.2 × 19.8	4400–6200	9	2	90	49
116	2002 Jun. 04	52 430.735	GH	2.5 × 6.0	3976–7305	15	2	90	114

^a Date 2000 Jul. 30,31 means average of data during two nights; for this case average JD is given.

Table B.2. Observed continuum, H β and H α fluxes. Columns: 1 – UT-Date; 2 – Julian date; 3 – a telescope code, according to Table 1; 4 – $F(\text{cont})$, the continuum flux at 5190 Å (in units of 10^{-15} erg s $^{-1}$ cm $^{-2}$ Å $^{-1}$), reduced to the 1 m telescope aperture $4.2'' \times 19.8''$; 5 – ε_c , the estimated continuum flux error; 6 – $F(\text{H}\beta)$, the H β total flux (in units of 10^{-13} erg s $^{-1}$ cm $^{-2}$); 7 – $\varepsilon_{\text{H}\beta}$, the H β flux error; 8 – $F(\text{H}\alpha)$, the H α total flux (in units of 10^{-13} erg s $^{-1}$ cm $^{-2}$); 9 – $\varepsilon_{\text{H}\alpha}$, the H α flux error.

UT-date	JD (2400 000+)	Code	$F(\text{cont})$ (5190) Å	ε	$F(\text{H}\beta)$ (4795–5018) Å	ε	$F(\text{H}\alpha)$ (6500–6800) Å	ε
1	2	3	4	5	6	7	8	9
1996 Jan. 14	50 097.570	L1			7.32	0.22	29.90	1.92
1996 Jan. 15	50 098.581	L1					32.74	2.10
1996 Feb. 14	50 127.579	L			8.26	0.24		
1996 Feb. 14	50 127.569	L					29.76	1.98
1996 Feb. 14	50 128.432	L			8.79	0.25		
1996 Feb. 14	50 128.472	L					32.81	2.18
1996 Mar. 19	50 162.382	L	14.13	1.03	7.85	0.08		
1996 Mar. 19	50 162.399	L					28.47	2.59
1996 Mar. 21	50 164.395	L	12.74	0.93	7.89	0.08		
1996 Mar. 21	50 164.412	L					25.04	2.28
1996 Jul. 10	50 275.283	L	16.98	0.51	10.04	0.30		
1996 Jul. 10	50 275.353	L					41.38	2.07
1997 Apr. 05	50 544.414	L1	10.83	0.63	7.67	0.38		
1997 Apr. 05	50 544.455	L1					36.69	1.83
1997 Apr. 08	50 547.331	L	11.75	0.68	7.14	0.36		
1997 Apr. 14	50 553.322	L	10.35	0.31	7.53	0.23		
1997 Apr. 14	50 553.330	L					37.53	.88
1998 Jan. 21	50 834.632	L	14.96	0.45	8.96	0.27		
1998 Jan. 21	50 834.639	L					34.65	1.73
1998 Feb. 23	50 867.535	L	14.36	0.43	10.16	0.30		
1998 Feb. 23	50 867.539	L					37.81	1.89
1998 Apr. 27	50 931.474	L1					42.10	1.68
1998 Apr. 30	50 934.438	L1					39.81: ^b	2.00
1998 Apr. 30	50 934.467	L1	18.49	0.55	9.98	0.30		
1998 May 04	50 938.289	L					36.98	1.85
1998 May 04	50 938.293	L	18.85	0.83	10.57	0.12		
1998 May 06	50 940.433	L	20.05	0.88	10.4	0.52		
1998 May 06	50 940.436	L					46.64:	5.6
1998 May 07	50 941.551	L	18.92	0.78	11.16	0.28		
1998 May 08	50 942.452	L	18.06	0.74	11.72	0.29		
1998 May 08	50 942.461	L	17.42	0.71	11.34	0.28		
1998 May 08	50 942.472	L					39.60	1.98
1998 Jun. 17	50 982.407	L1	17.52	0.18	11.42	0.23		
1998 Jun. 19	50 984.287	L1	17.26	0.17	11.74	0.23		
1998 Jun. 19	50 984.328	L1					44.45	1.68
1998 Jun. 20	50 985.281	L1					47.31	1.79
1998 Jun. 20	50 985.350	L1	18.44	:0.85	11.55	0.14		
1998 Jun. 25	50 990.409	L	16.41	0.10	11.90	0.17		
1998 Jun. 26	50 991.331	L	16.28	0.10	11.67	0.16		
1998 Jul. 14	51 008.778	GH	15.25	0.14	10.24	0.19	42.18	0.81
1998 Jul. 17	51 011.683	GH	15.05	0.14	10.52	0.20	43.35	0.84
1998 Jul. 26	51 020.703	GH	15.25	0.34	10.68	0.31	41.69	3.62

Table B.2. continued.

UT-date	JD (2 400 000+)	Code	$F(\text{cont})$ (5190) Å	ε	$F(\text{H}\beta)$ (4795–5018) Å	ε	$F(\text{H}\alpha)$ (6500–6800) Å	ε
1	2	3	4	5	6	7	8	9
1998 Jul. 27	51 021.712	GH	15.73	0.35	10.26	0.30	36.86	3.20
1999 Jan. 13	51 191.952	GH	13.78	0.21	9.41	0.10	32.40	1.04
1999 Jan. 14	51 193.011	GH	14.08	0.21	9.34	0.10	33.90	1.08
1999 Jan. 22	51 200.542	L1	13.46	0.40	9.44	0.28		
1999 Jan. 23	51 201.579	L1					34.24	1.10
1999 Jan. 25	51 203.565	L1	14.26	0.43	9.62	0.29		
1999 Jan. 26	51 204.576	L1					34.45	1.10
1999 Mar. 15	51 252.970	GH	15.63	0.47	8.57	0.26	38.69:	1.93
1999 Mar. 24	51 262.444	L1	16.59	0.16	10.03	0.16		
1999 Mar. 24	51 262.452	L1					36.17:	1.81
1999 Mar. 24	51 262.452	L	16.53	0.16	9.80	0.16		
1999 Apr. 11	51 279.533	L1	15.10	0.45	9.66	0.29		
1999 Jun. 12	51 342.409	L1	12.55	0.25	9.76	0.10		
1999 Jun. 14	51 344.354	L1	12.66	0.25	9.89	0.10		
1999 Jun. 16	51 346.335	L1	13.00	0.26	9.81	0.10		
1999 Jul. 16	51 376.277	L	14.06	0.42	10.12	0.30		
1999 Jul. 30	51 390.253	L1	10.98	0.33	8.36	0.25		
1999 Aug. 08	51 399.254	L1	10.43	0.31	8.76	0.26		
1999 Aug. 09	51 400.245	L1					35.52	1.78
2000 Jan. 10	51 553.567	L1	10.03	0.30	9.32	0.28		
2000 Jan. 27	51 570.959	GH	10.47	0.31	7.95	0.26	33.45	2.16
2000 Jan. 28	51 571.914	GH	12.52	0.38	7.59	0.25	36.64	2.36
2000 Feb. 14	51 588.510	L1	10.55	0.50	7.21	0.17		
2000 Feb. 15	51 589.506	L1	11.27	0.53	6.97	0.17		
2000 Feb. 26	51 600.898	GH	9.22	0.13	6.34	0.20	29.62	2.24
2000 Feb. 27	51 601.847	GH	9.40	0.13	6.63	0.21	26.60	2.02
2000 Mar. 14	51 618.483	L1	11.10	0.33	7.03	0.56		
2000 Mar. 15	51 619.478	L1	9.98	0.30	6.26	0.50		
2000 Apr. 01	51 636.414	L1	8.82	0.12	6.60	0.17		
2000 Apr. 04	51 639.397	L1	8.65	0.12	6.36	0.17		
2000 Apr. 25	51 659.839	GH	7.83	0.08	5.68	0.06	28.15	1.64
2000 Apr. 26	51 660.815	GH	7.73	0.08	5.63	0.06	25.95	1.52
2000 May 11	51 676.365	L1	8.59	0.26	5.22	0.16		
2000 May 16	51 681.283	L1					22.84	1.14
2000 May 20	51 685.321	L1					21.94	0.21
2000 May 21	51 686.258	L1	8.21	0.25	5.13	0.15		
2000 May 21	51 686.350	L1					22.24	0.21
2000 May 25	51 689.786	GH	8.13	0.08	5.35	0.18	22.54	0.72
2000 May 26	51 690.835	GH	8.12	0.08	5.07	0.15	23.59	1.18
2000 Jun. 06	51 702.378	L1	7.47	0.22	5.65	0.18		
2000 Jun. 08	51 704.299	L1	9.31	0.28	5.40	0.17		
2000 Jun. 15	51 711.308	L1					19.10	0.96
2000 Jun. 25	51 721.712	GH	8.09	0.24	5.07	0.15	18.09	0.90
2000 Jul. 12	51 738.335	L1					20.26	0.35
2000 Jul. 13	51 739.275	L1					19.76	0.35
2000 Jul. 28	51 754.269	L1	9.14	0.27	6.37	0.07		
2000 Jul. 29	51 755.301	L1	9.54	0.29	6.47	0.07		
2000 Jul. 30,31 ^a	51 756.786	L1	9.01	0.36	6.23	0.17		
2001 Jan. 25	51 935.482	L1	8.53	0.26	5.85	0.18		
2001 Jan. 26	51 936.517	L1					27.50	1.38

Table B.2. continued.

UT-date	JD (2 400 000+)	Code	$F(\text{cont})$ (5190) Å	ε	$F(\text{H}\beta)$ (4795–5018) Å	ε	$F(\text{H}\alpha)$ (6500–6800) Å	ε
1	2	3	4	5	6	7	8	9
2001 Jan. 29	51 938.560	L1	9.58	0.29	5.86	0.18		
2001 Feb. 03	51 944.498	L1	8.98	0.27	5.90	0.18		
2001 Feb. 16	51 957.492	L1	8.68	0.26	6.28	0.19		
2001 Mar. 13	51 981.867	GH	9.09	0.27	5.52	0.17	23.26	1.16
2001 Apr. 13	52 013.360	L1	8.85	0.27	4.28	0.13		
2001 Apr. 13	52 013.451	L1					21.00	1.05
2001 May 05	52 034.784	GH	7.71	0.23	3.52	0.11	17.85	0.89
2001 May 12	52 041.829	GH	7.98	0.08	3.32	0.04	14.97	0.72
2001 May 14	52 043.859	GH	7.94	0.08	3.34	0.04	16.01	0.77
2001 Jun. 14	52 074.772	GH	9.91	0.20	4.55	0.08	18.57	0.82
2001 Jun. 15	52 075.738	GH	9.64	0.19	4.44	0.07	17.45	0.77
2001 Jul. 10	52 101.367	L	11.27	0.11	6.36	0.22		
2001 Jul. 10	52 101.383	L					26.01	0.38
2001 Jul. 12	52 103.273	L					26.56	0.39
2001 Jul. 12	52 103.283	L	11.31	0.11	6.68	0.23		
2001 Jul. 21	52 112.340	L1	11.45	0.41	6.27	0.16		
2001 Jul. 22	52 113.261	L	10.65	0.38	6.56	0.17		
2001 Jul. 22	52 113.286	L					24.13	1.21
2001 Jul. 23	52 114.335	L1	11.13	0.40	6.28	0.16		
2001 Jul. 26	52 117.333	L1	10.72	0.30	6.49	0.15		
2001 Aug. 09	52 131.300	L1	10.54	0.32	4.95	0.15		
2002 May 15	52 410.456	L1	7.32	0.22	2.64	0.08		
2002 May 17	52 412.435	L1	8.11	0.24	2.64	0.08		
2002 Jun. 04	52 430.735	GH	7.41	0.22	2.42	0.07	13.70	0.68

^a Date 2000 Jul. 30,31 means average of data during two nights; for this case average JD is given.

^b Colon marks unsure value.